

GreedyPixel: Fine-Grained Black-Box Adversarial Attack Via Greedy Algorithm

Hanrui Wang*, Ching-Chun Chang, Chun-Shien Lu, Christopher Leckie, and Isao Echizen,

Abstract—Deep neural networks are highly vulnerable to adversarial examples, which are inputs with small, carefully crafted perturbations that cause misclassification—making adversarial attacks a critical tool for evaluating robustness. Existing black-box methods typically entail a trade-off between precision and flexibility: pixel-sparse attacks (e.g., single- or few-pixel attacks) provide fine-grained control but lack adaptability, whereas patch- or frequency-based attacks improve efficiency or transferability, but at the cost of producing larger and less precise perturbations. We present *GreedyPixel*, a fine-grained black-box attack method that performs *brute-force-style, per-pixel greedy optimization* guided by a surrogate-derived priority map and refined by means of query feedback. It evaluates each coordinate directly *without any gradient information*, guaranteeing monotonic loss reduction and convergence to a coordinate-wise optimum, while also yielding near white-box-level precision and pixel-wise sparsity and perceptual quality. On the CIFAR-10 and ImageNet datasets, spanning convolutional neural networks (CNNs) and Transformer models, GreedyPixel achieved state-of-the-art success rates with visually imperceptible perturbations, effectively bridging the gap between black-box practicality and white-box performance. The implementation is available at <https://github.com/azrealwang/greedypixel>.

Index Terms—Black-box adversarial attack, greedy algorithm.

I. INTRODUCTION

Deep neural networks have achieved state-of-the-art performance in vision, language, and multimodal tasks, yet they remain vulnerable to adversarial examples, which are inputs with small, carefully crafted perturbations that cause incorrect predictions. Adversarial attacks are therefore a critical tool for assessing model robustness, particularly in safety-critical applications such as face recognition [1], medical diagnosis [2], and multimodal reasoning [3]. Existing adversarial attacks can be characterized along four complementary dimensions, which together reveal the gap that this paper investigates.

Gradient access: The first dimension distinguishes whether attacks have access to model gradients. *White-box* attacks exploit exact gradients to efficiently solve the optimization problem [4]–[8]. These methods are highly effective and query-efficient but rely on access that is rarely available in

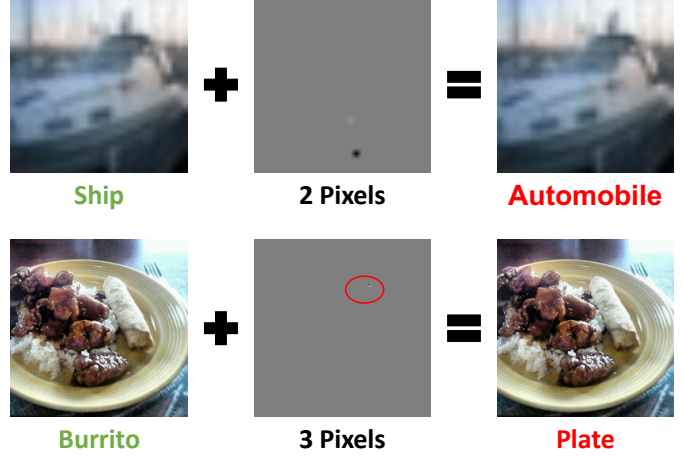


Fig. 1: Adversarial examples generated by GreedyPixel, which perturbs only a small, high-saliency subset of pixels. This approach preserves visual fidelity while achieving near white-box attack success rates using only black-box feedback.

deployed systems. *Black-box* attacks operate without gradients and instead rely on model outputs, making them more practical but typically less effective and less efficient.

Information source: The second dimension distinguishes the information source. Within black-box settings, attacks can be divided in accordance with the information they exploit. *Query-only* methods use label or score feedback from the target model [9]–[12]. They are flexible and require no additional models but converge slowly and incur a high query cost on high-resolution inputs, and they cannot be directly upgraded if white-box access becomes available. *Transfer-only* methods craft adversarial examples on surrogate models and transfer them to the target [19]–[24]; they are computationally efficient but suffer from limited transferability. *Query-and-transfer* methods combine surrogate guidance with query feedback [25]–[27], mitigating both issues by adapting to the target decision boundary. A key advantage of both transfer-only and query-and-transfer methods is that they can seamlessly leverage white-box information if it becomes available, improving efficiency and attack strength without changing the overall algorithmic framework.

Perturbation pattern: The third dimension distinguishes how perturbations are distributed across the image. *Pixel-wise or sparse* attacks [13], [14] modify only a small subset of pixels and can achieve high perceptual quality by concentrating changes on the most influential coordinates. In contrast, *block-*

* Corresponding author.

Hanrui Wang, Ching-Chun Chang, and Isao Echizen are with Echizen Lab, National Institute of Informatics (NII), Tokyo, Japan, e-mail: {hanrui_wang, ccchang, iechizen}@nii.ac.jp. Chun-Shien Lu is with Institute of Information Science, Academia Sinica, Taipei, Taiwan, e-mail: lcs@iis.sinica.edu.tw. Christopher Leckie is with the School of Computing and Information Systems, the University of Melbourne, Australia, e-mail: caleckie@unimelb.edu.au.

This work was partially supported by JSPS KAKENHI Grants JP21H04907 and JP24H00732, by JST CREST Grant JPMJCR20D3 and JPMJCR2562 including AIP challenge program, by JST AIP Acceleration Grant JP-MJCR24U3, and by JST K Program Grant JPMJKP24C2 Japan.

TABLE I: Related adversarial attacks and their characteristics.

Attack	Strategy	White-box	Black-box	High ASR	Minimal Changes	Direct Optimization
FGSM [4] [2014]	Gradient-based	✓	✗	✓	✗	✓
CW [5] [2017]	Gradient-based	✓	✗	✓	✓	✓
PGD [6] [2018]	Gradient-based	✓	✗	✓	✗	✓
GreedyFool [7] [2020]	Gradient-based	✓	✗	✓	✓	✓
APGD [8] [2020]*	Gradient-based	✓	✗	✓	✗	✓
AutoAttack [8] [2020]*	Ensembling white and black	✓	✗	✓	✗	✓
PBA [9] [2019]	Submodular searching	✗	✓	✓	✗	✓
Square Attack [10] [2020]	Submodular searching	✗	✓	✓	✗	✓
MGA [11] [2020]	Genetic algorithm	✓	✓	✓	✗	✓
MF-GA [12] [2021]	Genetic algorithm	✗	✓	✓	✗	✓
One-Pixel [13] [2019]	Pixel-wise	✗	✓	✗	✓	✓
BruSLe [14] [2024]*	Pixel-wise	✗	✓	✓	✓	✓
SSAH [15] [2022]	Frequency domain	✓	✓	✗	✓	✓
S ² I-FGSM [16] [2022]	Frequency domain	✓	✓	✗	✗	✓
Frequency-Aware [17] [2024]	Frequency domain	✓	✓	✗	✗	✓
N-HSALF [18] [2024]	Frequency domain	✗	✓	✗	✗	✓
FIA [19] [2021]	Transferable attack	✓	✓	✗	✗	✓
DeCoWA [20] [2024]*	Transferable attack	✓	✓	✗	✗	✓
OPS [21] [2025]*	Transferable attack	✓	✓	✗	✗	✓
GAA [22] [2025]*	Transferable attack	✓	✓	✗	✗	✓
LEA2 [23] [2023]	Transferable, Frequency	✓	✓	✗	✗	✓
MFI [24] [2024]	Transferable, Frequency	✓	✓	✗	✗	✓
BASES [25] [2022]	Query-and-transfer-based	✓	✓	✓	✗	✓
GFCS [26] [2022]*	Query-and-transfer-based	✓	✓	✓	✗	✓
SQBA [27] [2024]*	Query-and-transfer-based	✓	✓	✗	✗	✓
CG [28] [2022]	Generator-based	✓	✓	✓	✗	✗
MCG [29] [2023]*	Generator-based	✓	✓	✓	✗	✗
DifAttack [30] [2024]	Generator-based	✓	✓	✓	✗	✗
CDMA [31] [2024]	Generator-based	✓	✓	✓	✗	✗
GreedyPixel (Ours)	Query-and-transfer-based Pixel-wise Greedy algorithm	✓	✓	✓	✓	✓

*denotes attacks used for evaluation comparison in Section V. ASR denotes attack success rate.

or *region-based* attacks (e.g., Square Attack [10]) flip entire patches, which may be more query-efficient, but often produce visually perceptible artifacts and are less precise in localizing the minimal perturbation. *Frequency-domain attacks* [15]–[18], [23], [24] search for perturbations in the Fourier domain and can improve transferability by exploiting global spectral information, but they typically generate dense, image-wide perturbations that lack fine-grained spatial control and may reduce visual imperceptibility, especially in high-frequency regions where changes are more noticeable.

Optimization strategy: Finally, the fourth dimension distinguishes whether attacks require additional training. *Direct optimization* methods are training-free and iteratively refine perturbations on-the-fly, enabling immediate adaptation to new targets and threat models. *Training-dependent* approaches include generator-based attacks [28]–[31], which require large datasets and costly retraining and may overfit to the surrogate data distribution, reducing robustness under domain shift. While generator-based methods produce adversarial examples quickly after training, their training cost and inflexibility limit their applicability in real-time or data-constrained scenarios.

Taken together, these dimensions highlight a gap: no existing attack simultaneously achieves (i) query-and-transfer guidance, (ii) pixel-wise sparsity, and (iii) training-free direct optimization. To address this gap, we developed GreedyPixel, a fine-grained black-box attack method that combines a surrogate-derived pixel-priority map with greedy, per-pixel

optimization refined by query feedback. As illustrated in Figure 1, GreedyPixel perturbs only a small set of high-saliency pixels, achieving visually imperceptible yet highly successful attacks without requiring gradients.

As summarized in Table I, no prior method jointly satisfies the three criteria mentioned above. Query-only methods lack surrogate guidance and converge slowly; transfer-only methods cannot adapt to the target decision boundary; and generator-based methods require retraining and do not guarantee sparse perturbations. GreedyPixel unifies these three criteria, rendering brute-force-style per-pixel search practical and bridging the precision gap between white-box and black-box attacks.

Our contributions are summarized as follows:

- **Fine-grained brute-force optimization for black-box attacks.** We introduce a surrogate-guided, per-pixel greedy search that makes *brute-force-style* coordinate evaluation practical in black-box settings, delivering truly fine-grained perturbation control without gradient access.
- **White-box-level precision without gradients.** Our deterministic, coordinate-wise updates guarantee monotonic loss decrease and convergence to a local coordinate optimum, enabling precision comparable to white-box attacks while remaining fully training-free and black-box.
- **Comprehensive validation across architectures and threat models.** On the CIFAR-10 and ImageNet datasets, spanning convolutional neural networks (CNNs) and Transformers, GreedyPixel achieved state-of-the-art at-

tack success rates, sparser and less perceptible perturbations, and fast convergence, providing a practical framework for fine-grained robustness evaluation.

II. RELATED WORK

We review white-box and black-box attacks, summarizing their characteristics and challenges while comparing them with our proposed GreedyPixel method in Table I.

White-box attacks rely on full model knowledge and gradient access for perturbation generation. The Fast Gradient Sign Method (FGSM) [4] generates adversarial examples efficiently but often fails to find optimal perturbations. The Projected Gradient Descent (PGD) method [6] improves the attack success rate (ASR) through iterative refinement of the perturbation. The Auto PGD (APGD) method [8] adapts step sizes dynamically for better performance, while the Carlini & Wagner (CW) method [5] achieves higher visual quality at the cost of greater computation. The AutoAttack [8] method integrates multiple algorithms, including APGD. The GreedyFool [7] method uses a two-stage greedy strategy but still requires gradient access, whereas the GreedyPixel method uses a gradient-free greedy approach to identify effective perturbations. However, white-box attacks struggle in black-box scenarios due to the unavailability and non-transferability of gradients. Additionally, they often perturb all pixels, producing noticeable differences from the original images.

Black-box attacks generate adversarial examples through diverse strategies, such as single-pixel modification (One-Pixel [13]), submodular search (Square [10], Parsimonious Black-box Attack (PBA) [9]), and genetic algorithms (e.g., Momentum Gradient Attack (MGA) [11], Multiple Fitness Functions (MF-GA) [12]). The Feature Importance-aware Attack (FIA) [19], Deformation-Constrained Warping Attack (DeCoWA) [20], Orthogonal Projection Strategy (OPS) [21], and Ghost Adversarial Attack (GAA) [22] enhance adversarial example transferability, while methods such as Black-box Attack with Surrogate Ensemble Strategy (BASES) [25], GreedyFool Coordinate Search (GFCS) [26], and Small Query Black-box Attack (SQBA) [27] integrate surrogate gradients with query feedback and thereby achieve higher success rates. The Query-Efficient Score-Based Black-Box Sparse Adversarial Attack (BruSLe) [14] discovers sparse perturbations through Bayesian optimization.

Frequency-domain approaches (S^2I -FGSM [16], N -HSA_{LF} (HSA: harmonic spectrum alignment) [18], Frequency-Aware [17], SSAH (Semantic Similarity Attack on High-frequency components) [15]) modify spectral components to improve transferability. Recent methods such as LEA2 (Lightweight Ensemble Adversarial Attack (via Non-overlapping Vulnerable Frequency Regions)) [23] and MFI (Mixed-Frequency Input) [24] further exploit frequency subspaces by targeting non-overlapping vulnerable bands or by mixing frequency components across images, respectively, and achieve strong transfer results on both CNNs and Transformers. However, frequency-domain methods typically generate dense perturbations that are difficult to constrain for sparsity, and they cannot adapt to the target decision boundary without additional queries.

Generator-based methods (Conditional Generative Attack (CG) [28], Meta-learning-based Conditional Generator (MCG) [29], DifAttack [30], Conditional Diffusion Model Attack (CDMA) [31]) use learned feature spaces to generate adversarial examples with a single forward pass but require expensive retraining and may overfit to the training distribution.

Overall, existing black-box attacks face a high query cost, limited adaptability to white-box information, a lack of instance optimality, and weak control of perturbation sparsity; many rely on random search, gradient approximation, or region-/frequency-based sampling, which restricts precision. In contrast, *GreedyPixel* performs *brute-force-style, per-pixel greedy optimization* that directly evaluates each coordinate without gradients, thereby achieving precise fine-grained control. Coupled with a surrogate-driven pixel-priority map and query-refined updates, this design guarantees monotonic loss reduction, coordinate-wise convergence, and explicit sparsity control, thereby approaching the precision of gradient-based white-box methods while remaining fully black-box and training-free.

III. GREEDYPIXEL METHODOLOGY

This section presents the GreedyPixel attack methodology. Sections III-A and III-B define the threat models and problem formulation. Section III-C introduces the key design principles and underlying rationale, situating GreedyPixel among related attack families. The attack constructs a pixel-wise priority map (Section III-D) and iteratively processes pixels (Section III-E). Finally, the complete algorithm is summarized in Section III-F.

A. Threat Model

GreedyPixel is primarily designed for black-box attacks but adapts to white-box scenarios when gradient access is available. In black-box mode, it relies on query feedback, using a surrogate model to prioritize pixels. In white-box mode, it directly utilizes target model gradients, streamlining perturbation generation. Unlike most black-box attacks, GreedyPixel can transition to a white-box attack, as transfer-based methods allow this adaptation. Additionally, it operates without L_∞ -norm constraints, similar to sparse attacks like One-Pixel [13] and BruSLe [14]. GreedyPixel supports three threat models:

- White-box with constrained L_∞ -norm;
- Black-box with constrained L_∞ -norm;
- Black-box without L_∞ -norm constraints.

B. Adversary Goal and Loss Function

Adversarial attacks aim to manipulate predictions through subtle perturbations. Let x and y denote the original image and its ground-truth label, respectively, and let x' represent the adversarial example, formulated as

$$x' = x + \delta, \quad \text{s.t. } \|\delta\|_\infty \leq \epsilon, \quad (1)$$

where ϵ is the maximum allowable perturbation magnitude. Thus, given a loss function ℓ with respect to x' , the optimization objective in GreedyPixel to achieve misclassification is

$$x' = \arg \min_{x'} \ell(x'). \quad (2)$$

GreedyPixel utilizes the CW loss function [5] to define its optimization problem. The CW loss is designed to alter the prediction between the target and highest possible non-target label. For the misclassification scenario, the loss function used by GreedyPixel is formulated as

$$\ell(x') = Z(x')_y - \max_{i \neq y} Z(x')_i, \quad (3)$$

where $Z(x')$ represents the logits (pre-softmax activations) of the target model (for brevity, we use Z to refer to the target model), and y and i denote the indices, referring to labels. Specifically, $\ell \geq 0$ indicates a correct classification, while $\ell < 0$ indicates a successful misclassification attack.

C. Design Overview and Positioning

To clearly position GreedyPixel and highlight its novelty, we clarify its design principle and contrast it with related attacks. Our design is fundamentally motivated by brute-force search, which is optimal but computationally infeasible. The following discussion formalizes how we systematically reduce the complexity of brute-force search to a practical level and highlights the resulting algorithmic advantages.

a) Brute-force motivation: Brute-force is optimal but infeasible for practical image sizes. For an image of size $C \times H \times W$, the continuous perturbation space is unbounded:

$$Q_{\text{continuous}} = \mathcal{O}(\infty^{H \times W \times C}), \quad (4)$$

where each pixel may take infinitely many values. Restricting perturbations to the discrete range $\{-\epsilon, \dots, +\epsilon\}$ yields

$$\begin{aligned} Q_{\text{discrete}} &= \{-\epsilon, \dots, +\epsilon\}^{H \times W \times C} \\ &= (2 \times \text{int}(\epsilon \cdot 255) + 1)^{H \times W \times C}, \end{aligned} \quad (5)$$

where $\text{int}(\epsilon \cdot 255)$ denotes the maximum pixel change on a 1–255 scale, “2” accounts for \pm , and “+1” includes 0. Even if we restrict the perturbations to only the most extreme values ($-\epsilon$ and $+\epsilon$), the space remains exponential:

$$Q_{\text{binary}} = \{-\epsilon, +\epsilon\}^{H \times W \times C} = 2^{H \times W \times C}. \quad (6)$$

This binary restriction is justified. In our analysis of 1,000 adversarial examples generated by AutoAttack [8], 70.43% of the perturbations in L_∞ -norm attacks occurred at $\pm\epsilon$, confirming the importance of these extreme values. Therefore, GreedyPixel is designed as a principled reduction of brute-force search, focusing on $\pm\epsilon$ perturbations and systematically reducing complexity to a tractable pixel-wise form.

b) Fine-grained vs. coarse-grained search: We define *fine-grained* attacks as those that operate directly at the pixel level (e.g., PGD [6]), while *coarse-grained* attacks update regions or blocks (e.g., Square Attack [10]). Coarse-grained updates often lead to suboptimal perturbations because their search space $\mathcal{S}_{\text{coarse}}$ is a strict subset of the full pixel-wise space $\mathcal{S}_{\text{pixel}}$:

$$\mathcal{S}_{\text{coarse}} \subset \mathcal{S}_{\text{pixel}}. \quad (7)$$

Thus, even with infinite queries, coarse-grained search cannot guarantee global optimality. GreedyPixel, in contrast, deterministically exhausts the per-pixel candidate space in a fixed ordering. GreedyPixel is the first query-based black-box attack to implement a fine-grained brute-force strategy without gradient access.

c) Local exhaustive search vs. gradient-based local optima: Instead of enumerating all pixels jointly, GreedyPixel applies brute-force locally to each pixel in sequence. The per-pixel cost is

$$Q_{\text{pixel}} = \{-\epsilon, +\epsilon\}^C = 2^C, \quad (8)$$

which is trivial. Running over all pixels once (a one-pass search) requires

$$Q_{\text{one-pass}} = H \times W \times 2^C, \quad (9)$$

which transforms an exponential search into a linear-time procedure with respect to the number of pixels. This makes repeated passes computationally feasible even under query budgets (e.g., $Q_{\text{one-pass}} = 8192$ on CIFAR-10). Repeated passes approximate coverage of the full binary space Q_{binary} (Equation (6)) in a sequential manner. Unlike gradient-based attacks (e.g., CW [5], PGD [6]), which may become trapped in local minima due to following a fixed gradient direction [32], [33], GreedyPixel guarantees local optimality at each per-pixel update and empirically converges towards solutions close to the global optimum with repeated passes.

d) Surrogate-guided ordering: Although pixel-wise exhaustive search is feasible, iterating over all pixels uniformly is inefficient under query constraints. To accelerate convergence, GreedyPixel leverages a surrogate model to prioritize pixels in accordance with their importance. We specifically use adversarially trained surrogates that emphasize robust, semantically meaningful features such as object edges and textures rather than spurious background correlations [34]. Perturbations placed on these high-saliency regions are less perceptually noticeable than those on flat backgrounds, aligning with evidence from human perception that distortions are masked in textured regions. Our ablation confirms that adversarially trained surrogates outperform non-robust surrogates and random orderings in both efficiency and perceptual quality.

e) Training-free optimization: GreedyPixel is training-free and iteratively refines perturbations in input space, guaranteeing immediate applicability to any new model or threat setting. This strategy is highly flexible and naturally supports both targeted and untargeted objectives. By operating directly on model outputs, it avoids overfitting and remains robust even when the target model distribution differs from that of any surrogate or auxiliary dataset.

In contrast, training-dependent approaches include generator-based attacks and learned surrogates [28]–[31]. While they can generate adversarial examples with a single forward pass at inference time, they require substantial labeled data and computational resources for training, and must also be retrained whenever the target model or task changes. This additional retraining overhead makes them impractical in dynamic or online settings where the model evolves or defenses are updated.

Moreover, generators optimize an expected loss over the training distribution and cannot guarantee per-instance optimality, often resulting in suboptimal perturbations or reduced transferability under distribution shift. In addition, their dense, image-wide perturbations make it challenging to enforce sparsity constraints or guarantee visual imperceptibility, whereas

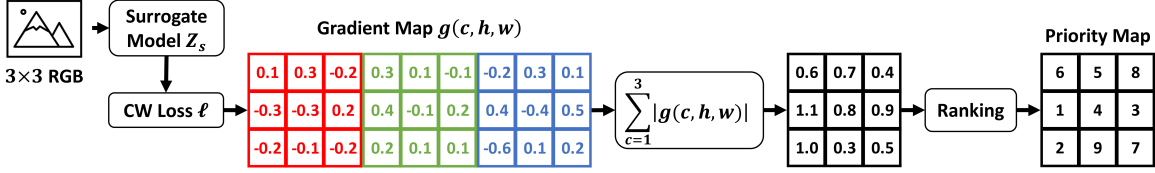


Fig. 2: Pixel-wise priority map obtained by ranking gradient g of the CW loss function ℓ with respect to input x and ground-truth label y within a surrogate model Z_s . Replacing the surrogate model with the target model yields a white-box attack.

direct optimization can explicitly control sparsity at the level of individual pixels.

These limitations motivate our adoption of direct, training-free optimization, an approach that is inherently adaptable, data-efficient, and theoretically grounded in a coordinate-wise greedy search strategy.

f) Comparison to prior work:

- **Gradient-based white-box attacks** (e.g., CW [5], PGD [6]) follow gradients and thus risk getting trapped in local minima; GreedyPixel avoids this through exhaustive per-pixel updates.
- **Greedy algorithms** (e.g., GreedyFool [7]) greedily select pixel subsets for gradient descent and thus remain gradient-dependent. GreedyPixel dispenses with gradients entirely.
- **Pixel-wise attacks** (e.g., One-Pixel [13], BruSLe [14]) operate at the pixel level but search a restricted perturbation space. GreedyPixel evaluates all 2^C channel perturbations, covering a superset of states.
- **Transfer-based attacks** (e.g., DeCoWA [20]) are query-free but lack robustness when faced with surrogate–target mismatch. GreedyPixel actively adapts through queries and thereby achieves stronger success rates.
- **Random-search attacks** (e.g., Square Attack [10]) perturb coarse blocks stochastically and explore only a restricted subset of the pixel-wise space.
- **Generator-based attacks** (e.g., MCG [29]) enable fast inference after training but require substantial labeled data and retraining for each new target, do not guarantee per-instance optimality, and struggle to enforce sparsity or maintain visual imperceptibility under distribution shift.

Together, these differences establish GreedyPixel as the first practical, query-based, fine-grained brute-force attack method that is both robust and perceptually aware.

Takeaway

GreedyPixel performs local exhaustive pixel-wise search guided by surrogate-based prioritization and refined through query feedback. This approach (i) reduces brute-force search to linear time, (ii) avoids gradient-based local minima, (iii) concentrates perturbations on robust, semantically meaningful pixels to preserve visual quality, and (iv) is training-free, eliminating generator retraining costs while remaining directly upgradeable to white-box settings.

Algorithm 1 Pixel-Wise Priority Map

Require: Original image x of size $C \times H \times W$ with ground-truth label y and surrogate model Z_s .

Ensure: Priority map $\{(h_i, w_i)\}_{i=1}^{H \times W}$.

- 1: $\ell(x) = Z_s(x)_y - \max_{i \neq y} Z_s(x)_i$
- 2: $g(c, h, w) = \nabla_x \ell(x)$ \triangleright gradient map
- 3: $g'(h, w) = \sum_{c=1}^C |g(c, h, w)|$ \triangleright pixel importance
- 4: $\{(h_i, w_i)\}_{i=1}^{H \times W} = \text{Sort}(g'(h, w))_{\text{desc}}$
- 5: **return** $\{(h_i, w_i)\}_{i=1}^{H \times W}$

D. Pixel-Wise Priority Map

The pixel-wise priority map determines the order in which pixels are updated by GreedyPixel and is computed entirely on the basis of the surrogate model Z_s (used interchangeably for model and logits). Each pixel's priority is derived from the gradient of the CW loss ℓ with respect to input x , so pixels with the greatest potential saliency are perturbed first. Because this process relies only on Z_s , it requires no queries to the target model. When Z_s equals the target model (white-box), the same ordering yields the fastest convergence, and early stopping minimizes the number of manipulated pixels.

As shown in Figure 2, the priority map is generated as:

- *Step 1:* Compute $g(c, h, w) = \nabla_x \ell(x)$ on Z_s , where c, h, w denote channel, height, and width.
- *Step 2:* Aggregate per-pixel importance $g'(h, w) = \sum_{c=1}^C |g(c, h, w)|$.
- *Step 3:* Sort pixels by $g'(h, w)$ in descending order to form the update sequence.

Algorithm 1 summarizes the procedure.

Theoretical Rationale. We formalize the advantages of using a priority map by means of three complementary arguments:

a) Coverage without redundancy: Let H and W denote the image height and width, respectively, so the total number of pixel positions is $M = H \times W$. If pixel positions are sampled uniformly with *replacement*, the expected number of selections required to visit all M positions at least once (one-pass) is given by the coupon collector result [35]:

$$\mathbb{E}[\text{one-pass}] = M \cdot H_M \approx M \ln M, \quad (10)$$

where H_M is the M -th harmonic number $H_M = \sum_{k=1}^M \frac{1}{k}$. This shows that many queries are wasted revisiting pixels before one-pass coverage is achieved. By contrast, any fixed priority map (even a random but fixed permutation of the M

pixels) guarantees coverage in exactly M steps, eliminating redundancy and ensuring that each pixel is processed exactly once per pass.

b) *White-box optimality*: Let $g(p) = \nabla_{x_p} \ell(x)$ denote the gradient of the loss ℓ with respect to pixel p for RGB values ($p \in \{1, \dots, M\}$), and let $g_s(p)$ be the corresponding gradient on the surrogate model Z_s . When the surrogate matches the target (*i.e.*, $Z_s = Z$), we have $g_s(p) = g(p)$ for all pixels, and ranking pixels by $\|g_s(p)\|_1$ corresponds to performing steepest coordinate descent on the target loss. The locally optimal update for a single pixel (by first-order Taylor expansion) yields approximately

$$\Delta\ell_p \approx -\epsilon\|g(p)\|_1 = -\epsilon\|g_s(p)\|_1. \quad (11)$$

Processing pixels in descending order of $\|g_s(p)\|_1$ therefore achieves the maximum per-step loss reduction and yields the fastest convergence. Early stopping once misclassification is achieved further minimizes the number of perturbed pixels.

c) *Surrogate quality and perceptual benefit*: When $Z_s \neq Z$, ranking pixels by $\|g_s(p)\|_1$ remains superior to random selection as long as the surrogate and target pixel-wise gradients are positively aligned. We define their cosine similarity at pixel p as

$$\cos\theta_p = \frac{g_s(p)^\top g(p)}{\|g_s(p)\|_2 \|g(p)\|_2}. \quad (12)$$

If $\cos\theta_p > 0$, the target-loss reduction per-pixel update tends to increase with

$$-\Delta\ell_p \propto \epsilon \cdot \rho_p \cdot \|g_s(p)\|_1, \quad (13)$$

where $\rho_p = \cos\theta_p$ quantifies the alignment at pixel p . Thus, pixels with larger $\|g_s(p)\|_1$ are expected to yield greater loss reduction on the target, even when $Z_s \neq Z$.

Adversarially trained surrogates increase ρ_p because they produce gradients that emphasize robust, semantically meaningful features such as object edges and textures [34]. Prioritizing these regions benefits both attack performance and perceptual quality: it improves ASR by perturbing genuinely predictive features while reducing perceptual distortion because perturbations are placed on visually complex regions rather than smooth backgrounds, thereby aligning with texture-masking effects in human vision.

Takeaway

The pixel-wise priority map is theoretically grounded in three complementary properties: (*i*) it guarantees efficient one-pass coverage without redundant queries; (*ii*) it achieves optimal convergence speed when the surrogate matches the target; (*iii*) it remains superior to random ordering even when the surrogate and target do not match by prioritizing robust, semantically meaningful pixels. Together, these properties result in faster attacks and visually subtler adversarial examples.

Algorithm 2 Greedy Strategy for a Single Pixel (with Query Feedback)

Require: Image x of size $C \times H \times W$, current perturbation $\delta^{(t)}$, selected pixel p , target model Z , loss function $\ell(\cdot)$, perturbation set $\{-\epsilon, +\epsilon\}$.

Ensure: Updated perturbation $\delta^{(t+1)}$, updated loss $\ell^{(t+1)}$.

```

1:  $\delta_{-p}^{(t)} = \delta^{(t)} - \mathcal{I}_p(\delta^{(t)})[p]$   $\triangleright$  zero out current pixel
2: for each  $\delta_p \in \{-\epsilon, +\epsilon\}^C$  do
3:    $\tilde{\delta} = \delta_{-p}^{(t)} + \mathcal{I}_p(\delta_p)$ 
4:    $\ell_{\delta_p} = \ell(x + \tilde{\delta})$ 
5: end for
6:  $\hat{\delta}_p = \arg \min_{\delta_p} \ell_{\delta_p}$   $\triangleright$  select optimal candidate
7: if  $\ell_{\hat{\delta}_p} < \ell(x + \delta^{(t)})$  then  $\triangleright$  accept if loss decreases
8:    $\delta^{(t+1)} = \delta_{-p}^{(t)} + \mathcal{I}_p(\hat{\delta}_p)$ 
9: else
10:    $\delta^{(t+1)} = \delta^{(t)}$   $\triangleright$  reject, keep unchanged
11: end if
12:  $\ell^{(t+1)} = \ell(x + \delta^{(t+1)})$ 
13: return  $\delta^{(t+1)}, \ell^{(t+1)}$ 

```

E. Pixel-Wise Greedy Algorithm

This subsection introduces the core mechanism of GreedyPixel. We first present the per-pixel greedy update rule, then show how score-based query feedback ensures a monotonic decrease in the target loss, and finally analyze convergence and its connection to global optimality.

1) *Greedy Update Rule*: Let $\delta^{(t)} \in \mathbb{R}^{C \times H \times W}$ denote the full perturbation tensor at iteration t , so that

$$x^{(t)} = x + \delta^{(t)}. \quad (14)$$

At each step, a pixel $p = (h, w)$ is selected from the priority map produced by Algorithm 1. Let $\delta^{(t)}[p] \in \mathbb{R}^C$ denote the current C -dimensional perturbation vector at p , and define the zeroed perturbation as

$$\delta_{-p}^{(t)} = \delta^{(t)} - \mathcal{I}_p(\delta^{(t)})[p], \quad (15)$$

where $\mathcal{I}_p(\cdot)$ embeds a C -channel vector at pixel p (zeros elsewhere). The algorithm exhaustively enumerates all 2^C candidate vectors $\delta_p \in \{-\epsilon, +\epsilon\}^C$ and selects

$$\hat{\delta}_p = \arg \min_{\delta_p \in \{-\epsilon, +\epsilon\}^C} \ell(x + \delta_{-p}^{(t)} + \mathcal{I}_p(\delta_p)). \quad (16)$$

The pixel update is applied in accordance with

$$\delta^{(t+1)} = \delta_{-p}^{(t)} + \mathcal{I}_p(\hat{\delta}_p), \quad x^{(t+1)} = x + \delta^{(t+1)}. \quad (17)$$

Thus, each iteration perturbs exactly one pixel with the locally optimal choice, leaving all other pixels fixed. The complete procedure for the greedy strategy at a single pixel is provided in Algorithm 2.

2) *Score-Based Query Feedback*: Surrogate-target alignment may be imperfect (*e.g.*, robust surrogate vs. non-robust target), and relying purely on surrogate ordering can yield poor transferability, as evidenced by DeCoWA results [20]

(Tables II to V). GreedyPixel mitigates this by incorporating *score-based query feedback*: the candidate update $\hat{\delta}_p$ is committed only if it strictly reduces the target loss,

$$\ell(x + \delta_{-p}^{(t)} + \mathcal{I}_p(\hat{\delta}_p)) < \ell(x^{(t)}). \quad (18)$$

Otherwise, the pixel is left unchanged ($\delta^{(t+1)} = \delta^{(t)}$, Step 10 of Algorithm 2). This constitutes an exact coordinate-descent step with a discrete line search along coordinate p . Because each accepted update reduces the loss, $\{\ell(x^{(t)})\}$ is monotonically non-increasing and therefore convergent.

Why surrogate ordering + feedback outperforms transfer-only? A purely transfer-based attack relies on the assumption of positive alignment,

$$\cos \theta_p = \frac{g_s(p)^\top g(p)}{\|g_s(p)\|_2 \|g(p)\|_2} > 0, \quad (19)$$

so that $\text{sign}(g_s(p))$ serves as a reliable proxy for $\text{sign}(g(p))$. When $\cos \theta_p$ is near zero or negative, the surrogate may produce harmful updates that increase the loss [34]. Target model feedback corrects instances of misalignment by rejecting such updates, while preserving effective updates under strong surrogate–target alignment (Steps 7–11 of Algorithm 2). Thus, combining surrogate ordering with target feedback yields efficiency when alignment is strong and robustness when the surrogate and target are mismatched.

Takeaway

Score-based feedback enables GreedyPixel to act as an adaptive algorithm that guarantees a monotonic decrease in the target loss. Surrogate ordering enables it to achieve fast convergence when alignment is strong and robust performance when alignment is weak, resulting in a higher ASR and lower perceptual distortion within the same query budget.

3) *Convergence and Global Optimality Approximation:* After one full pass over all $M = H \times W$ pixels, no single-pixel flip can further reduce the loss:

$$\ell(x^{(T+1)}) \leq \ell(x^{(T)} + \mathcal{I}_p(\delta_p)), \quad \forall p, \delta_p \in \{-\epsilon, +\epsilon\}^C. \quad (20)$$

Thus, $x^{(T+1)}$ is a coordinate-wise local minimum in the discrete space $\{-\epsilon, +\epsilon\}^{C \times M}$. Repeated passes progressively refine the solution, and, as $T \rightarrow \infty$, the algorithm approaches a deeper coordinate-wise minimum; empirically, this is often close to the global optimum of the discrete space.

Avoidance of gradient-based local minima. Gradient-based attacks such as PGD [6] update all pixels jointly:

$$x^{(t+1)} = x^{(t)} - \alpha \cdot \text{sign}(\nabla_x \ell(x^{(t)})). \quad (21)$$

On rugged loss landscapes, $\nabla_x \ell$ may vanish or guide the optimization into suboptimal local basins, causing premature convergence [32], [33]. GreedyPixel circumvents this pitfall by exhaustively evaluating candidate flips for each pixel, ensuring every accepted update strictly reduces the loss. As illustrated in Figure 3, GreedyPixel achieves lower loss than PGD and GreedyFool* even under an identical pixel-selection budget.

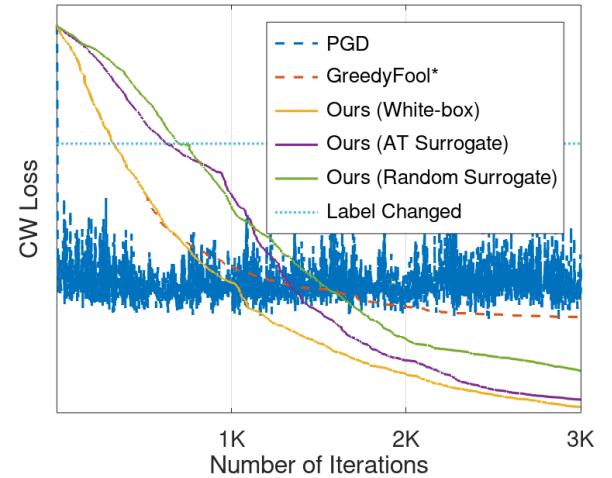


Fig. 3: CW loss vs. number of iterations for PGD [6], GreedyFool*, and GreedyPixel variants. GreedyFool* uses GreedyFool’s pixel-selection heuristic (top-50% salient pixels) [7] but replaces its gradient-descent update with a pixel-wise exhaustive search, ensuring a fair comparison under black-box assumptions. However, GreedyFool* converges to a higher loss plateau, revealing the limitations of its pixel-selection strategy. GreedyPixel achieves the lowest final loss, with white-box access converging fastest, followed by adversarially trained (AT) surrogate and random surrogate settings. The dotted line indicates the first-iteration label change.

Takeaway

GreedyPixel converges monotonically, achieves coordinate-wise optimality after each pass, and asymptotically approaches the global optimum. Unlike PGD, it is not susceptible to traps from local gradient directions and thus remains effective even on rugged, non-smooth loss landscapes.

F. Full Pipeline of GreedyPixel Attack

Throughout its iterations, GreedyPixel (Algorithm 3) processes pixels in accordance with the priority map (Algorithm 1) and applies the greedy update rule with query feedback (Algorithm 2). Additionally, the pixel-priority order may be refreshed periodically every N iterations to concentrate queries on the most promising coordinates while keeping the perturbation sparse. The attack terminates when either (i) the maximum query budget is reached, $t \cdot 2^C \leq Q_{\max}$, or (ii) misclassification is achieved, $\ell(x^{(t)}) < 0$.

The total query cost is thus

$$Q_{\text{Greedy}} = t \times 2^C \leq Q_{\max}, \quad (22)$$

where $2 = |\{-\epsilon, +\epsilon\}|$. This illustrates the efficiency of GreedyPixel relative to brute-force search ($2^{C \times H \times W}$ evaluations, Equation (6)). When $t \geq H \times W$, every pixel has been processed at least once. Thus, the number of manipulated pixels is $\min(t, H \times W)$, which scales with image resolution and directly corresponds to the query cost.

Algorithm 3 GreedyPixel Attack (Full Pipeline)

Require: Input x of size $C \times H \times W$, label y , target model Z , surrogate model Z_s , maximum perturbation ϵ , maximum query budget Q_{\max} , priority-map refresh period N .

- 1: $\delta^{(0)} = \mathbf{0}$, $t = 0$
- 2: **while** $t \cdot 2^C \leq Q_{\max}$ **do**
- 3: **if** $t \bmod N = 0$ **then**
- 4: $\{p_i\}_{i=1}^{H \times W} = \text{Algorithm 1}(x, y, Z_s)$ ▷ refresh priority map
- 5: **end if**
- 6: $p = p_{(t \bmod H \times W)}$
- 7: $\delta^{(t+1)}, \ell^{(t+1)} = \text{Algorithm 2}(x, y, Z, p, \delta^{(t)}, \epsilon)$
- 8: **if** $\ell^{(t+1)} < 0$ **then**
- 9: **break**
- 10: **end if**
- 11: $t \leftarrow t + 1$
- 12: **end while**
- 13: **return** $x' = x + \delta^{(t+1)}$

IV. EXPERIMENT SETTINGS**A. Datasets, Target, and Surrogate Models**

Attacks were evaluated on the CIFAR-10 [36] (32×32) and ImageNet [37] datasets (cropped to 64×64 and 224×224 for specific studies), each with 1,000 examples. The target models included four non-robust pretrained models: WideResNet-28-10 [38] for CIFAR-10, and ResNet-50 [38], ViT-Base-Patch16 [39], and VGG19-BN [40] for ImageNet. The inclusion of the Vision Transformer model (ViT-Base-Patch16) enabled a direct assessment of GreedyPixel on a non-CNN architecture and illustrates its generalizability beyond convolutional networks. Three robust models were also tested: WideResNet-28-10 [41], WideResNet-82-8 [42], and XCiT-S12 [43].

Ablation studies were conducted using various surrogate models [44]–[49], with fairness ensured by using the same surrogate model across attacks. In black-box settings, the surrogate differed from the target, while in white-box settings, they were identical. GreedyPixel utilized adversarially pretrained surrogate models for improved visual quality, whereas non-adversarial surrogate models were approximated using random sequences.

B. Benchmarks and Experimental Settings

The proposed GreedyPixel method was benchmarked against leading adversarial attack techniques under the three threat models described in Section III-A, with specific attacks selected from various strategies summarized in Table I.

White-box attacks with constrained L_∞ -norm distance (i.e., limited ϵ): GreedyPixel was compared with state-of-the-art gradient-based white-box attacks, including AutoAttack [8] and APGD [8], under a uniform perturbation constraint of $\epsilon = 4/255$. In this evaluation, the number of queries was left unrestricted.

Black-box attacks with constrained L_∞ -norm distance (i.e., limited ϵ): GreedyPixel was evaluated against several prominent black-box attack methods, including DeCoWA

[20] (purely transfer-based), GFCS [26] (score-and-transfer-based), MCG [29] (generator-based), SQBA [27] (score-and-transfer-based), and two recent attack methods (OPS [21] and GAA [22]), all under the same $\epsilon = 4/255$ constraint. The methods were evaluated under a maximum query budget of 20,000.

Black-box attacks with unconstrained L_∞ -norm distance (i.e., unlimited ϵ): For this setting, we compared GreedyPixel with a state-of-the-art sparse attack method, BruSLe [14], which has shown superior ASRs compared with previous methods like One-Pixel attack [13]. BruSLe's sparsity was fixed at 1% (10 pixels) for CIFAR-10 and 0.1% (50 pixels) for ImageNet, with both methods operating under a maximum query budget of 20,000.

Against adversarial defenses: The attacks were further evaluated against established adversarial defense mechanisms, including a state-of-the-art adversarial purification method, DiffPure [50], three recent adversarial training (AT) defenses [41]–[43], and one adversarial detection method [51], across all three threat models.

C. Evaluation Metrics

The evaluation metrics included several key aspects to assess the performance of the proposed attack and benchmark methods. An attack's effectiveness was measured by its ASR, with higher values indicating greater success in manipulating model predictions. Visual quality was assessed using the Structural Similarity Index Measure (SSIM) [52] and Learned Perceptual Image Patch Similarity (LPIPS) [53], where higher SSIM and lower LPIPS values indicate subtler deviations from the original images. Computational efficiency was measured by execution time, with shorter durations indicating more efficient attacks. The average number of queries (Avg. Q) reflected query efficiency, with fewer queries indicating better resource utilization. The adversarial detection rate quantified the proportion of adversarial examples identified as threats and was included as part of the assessment of attacks against adversarial defenses. A lower detection rate indicates greater attack effectiveness, reflecting better evasion of detection.

D. Implementation

GreedyPixel was implemented using the Adversarial Robustness Toolbox [54], with RobustBench [38] serving as the benchmark for evaluating adversarial robustness. The experiments were conducted on a workstation equipped with an NVIDIA A100 40-GB GPU.

V. PERFORMANCE**A. Attack Effectiveness**

We evaluated the GreedyPixel attack method and benchmarked its performance against state-of-the-art methods across three threat models (refer to Section IV-B). As summarized in Tables II to V, GreedyPixel consistently achieved higher ASRs than the benchmarks under the same conditions. White-box GreedyPixel attacks outperformed their black-box counterparts, which were constrained by a limited query budget.

TABLE II: Attack performance of WideResNet-28-10 [38] evaluated on CIFAR-10 [36].

Threat Model	Attack	Time(s)↓	Avg. Q↓	ASR(%)↑	LPIPS↓	SSIM↑
White-box (Limited ϵ)	APGD	1.7		100.0	0.0006	0.981
	AutoAttack	1.7	∞	100.0	0.0006	0.982
	Ours	1.3		100.0	0.0001	0.994
Black-box (Limited ϵ)	DeCoWA*	28.1	0	8.7	0.0022	0.986
	OPS	16.1	0	8.2	0.0028	0.990
	GAA	3.0	0	12.2	0.0022	0.986
	MCG	3.7	745	99.5	0.0013	0.978
	SQBA*	81.3	17,418	13.0	0.0016	0.988
	Ours	1.8	1,997	100.0	0.0002	0.995
Black-box (Unlimited ϵ)	BruSLe	1.4	367	98.7	0.0168	0.876
	Ours	0.3	318	100.0	0.0023	0.964

*DeCoWA [20] and SQBA [27] exhibited limited transferability when there was a significant discrepancy between the surrogate model (PreActResNet-18 [44]) and the target model (WideResNet-28-10 [38]). To ensure the correctness of our implementation, we evaluated their performance in a white-box attack setting (where the surrogate and target models are identical), achieving success rates of 70.5% and 84.3%, respectively. **Bold** indicates superior performance.

TABLE III: Attack performance of ResNet-50 [38] evaluated on ImageNet [37].

Threat Model	Attack	Time(s)↓	Avg. Q↓	ASR(%)↑	LPIPS↓	SSIM↑
White-box (Limited ϵ)	APGD	2.5		99.9	0.0351	0.954
	AutoAttack	2.6	∞	100.0	0.0343	0.955
	Ours	23.2		100.0	0.0006	0.997
Black-box (Limited ϵ)	DeCoWA*	536.3	0	8.0	0.0356	0.944
	OPS	60.1	0	16.1	0.0233	0.976
	GAA	11.5	0	19.5	0.0284	0.966
	GFCS	259.1	12,217	42.2	0.0229	0.978
	SQBA*	101.4	15,538	21.6	0.0224	0.971
	Ours	26.1	13,152	60.0	0.0002	≈ 1
Black-box (Unlimited ϵ)	BruSLe	7.2	913	98.0	0.0616	0.977
	Ours	2.0	980	99.9	0.0232	0.985

*DeCoWA [20] and SQBA [27] exhibited limited transferability when there was a significant discrepancy between the surrogate model (ConvNeXt [47]) and the target model (ResNet-50 [38]). To ensure the correctness of our implementation, we evaluated their performance in a white-box setting (where the surrogate and target models are identical), achieving success rates of 94.9% and 99.6%, respectively. **Bold** indicates superior performance.

Additionally, GreedyPixel demonstrated greater effectiveness on a low-resolution dataset (CIFAR-10) than on a high-resolution one (ImageNet) in the black-box setting as only a subset of pixels could be modified within a restricted query budget, thereby limiting attack success. Furthermore, as shown in Table IV, GreedyPixel maintained high ASRs and strong perceptual quality on ViT-Base-Patch16, confirming that the proposed approach is effective across both CNN- and Transformer-based models.

B. Attack Efficiency

We assessed the efficiency of the GreedyPixel attack method from two perspectives: execution time and query efficiency. As shown in Tables II to V, GreedyPixel outperformed all black-box attacks in execution time, making it the fastest method. Although it required more queries than query-based attacks such as DeCoWA [20], GFCS [26], and MCG [29], it achieved superior ASRs, lower execution times, and better visual quality (higher SSIM, lower LPIPS). This is due to

TABLE IV: Attack performance of ViT-Base-Patch16 (Vision Transformer) [39] evaluated on ImageNet [37].

Threat Model	Attack	Time(s)↓	Avg. Q↓	ASR(%)↑	LPIPS↓	SSIM↑
White-box (Limited ϵ)	APGD	2.6		100.0	0.0349	0.958
	AutoAttack	2.6	∞	100.0	0.0333	0.959
	Ours	63.4		100.0	0.0013	0.995
Black-box (Limited ϵ)	DeCoWA*	536.3	0	3.8	0.0356	0.944
	OPS	60.1	0	6.4	0.0233	0.976
	GAA	11.5	0	9.0	0.0284	0.966
	GFCS	347.3	15,769	24.0	0.0239	0.978
	SQBA*	112.3	18,024	9.6	0.0240	0.951
	Ours	65.0	16,096	37.8	0.0004	0.999
Black-box (Unlimited ϵ)	BruSLe	10.4	1,509	98.6	0.0641	0.977
	Ours	6.6	1,620	100.0	0.0341	0.978

*DeCoWA [20] and SQBA [27] exhibited limited transferability when there was a significant discrepancy between the surrogate model (ConvNeXt [47]) and the target model (ViT-Base-Patch16 [39]). To ensure the correctness of our implementation, we evaluated their performance in a white-box attack setting (where the surrogate and target models are identical), achieving success rates of 78% and 83.1%, respectively. **Bold** indicates superior performance.

TABLE V: Attack performance of VGG19-BN [40] evaluated on ImageNet [37].

Threat Model	Attack	Time(s)↓	Avg. Q↓	ASR(%)↑	LPIPS↓	SSIM↑
White-box (Limited ϵ)	APGD	0.8		100.0	0.0254	0.964
	AutoAttack	0.9	∞	100.0	0.0246	0.965
	Ours	26.2		100.0	0.0012	0.996
Black-box (Limited ϵ)	DeCoWA*	536.3	0	36.6	0.0356	0.944
	OPS	60.1	0	48.4	0.0233	0.976
	GAA	11.5	0	47.6	0.0284	0.966
	GFCS	125.0	6,198	71.5	0.0124	0.984
	SQBA*	39.4	9,846	50.1	0.0162	0.978
	Ours	13.2	6,662	84.7	0.0001	≈ 1
Black-box (Unlimited ϵ)	BruSLe	1.9	391	99.3	0.0580	0.978
	Ours	1.0	477	99.9	0.0111	0.993

*DeCoWA [20] and SQBA [27] exhibited limited transferability when there was a significant discrepancy between the surrogate model (ConvNeXt [47]) and the target model (VGG19-BN [40]). To ensure the correctness of our implementation, we evaluated their performance in a white-box setting (where the surrogate and target models are identical), achieving success rates of 99.2% and 99.9%, respectively. **Bold** indicates superior performance.

GreedyPixel's ability to compute eight queries in parallel ($\{-\epsilon, +\epsilon\}^3 = 8$), whereas other attacks query sequentially. Additionally, when the L_∞ -norm constraint (ϵ) was relaxed, GreedyPixel surpassed the attack efficiency of a state-of-the-art sparse attack, BruSLe [14].

The complexity of attacking high-resolution images (ImageNet) increases more sharply for GreedyPixel than for low-resolution images (CIFAR-10). Despite this, GreedyPixel achieved a 100% ASR for white-box attacks on CIFAR-10, outperforming methods such as APGD [8] and AutoAttack [8] in execution time. However, when applied to ImageNet, GreedyPixel remained effective but was less efficient in execution time than APGD and AutoAttack, reflecting the trade-off between resolution and computational cost.

C. Visual Quality

We computed the SSIM and LPIPS scores between the original inputs and adversarial examples to assess the visibility of adversarial perturbations. Additionally, we visualized

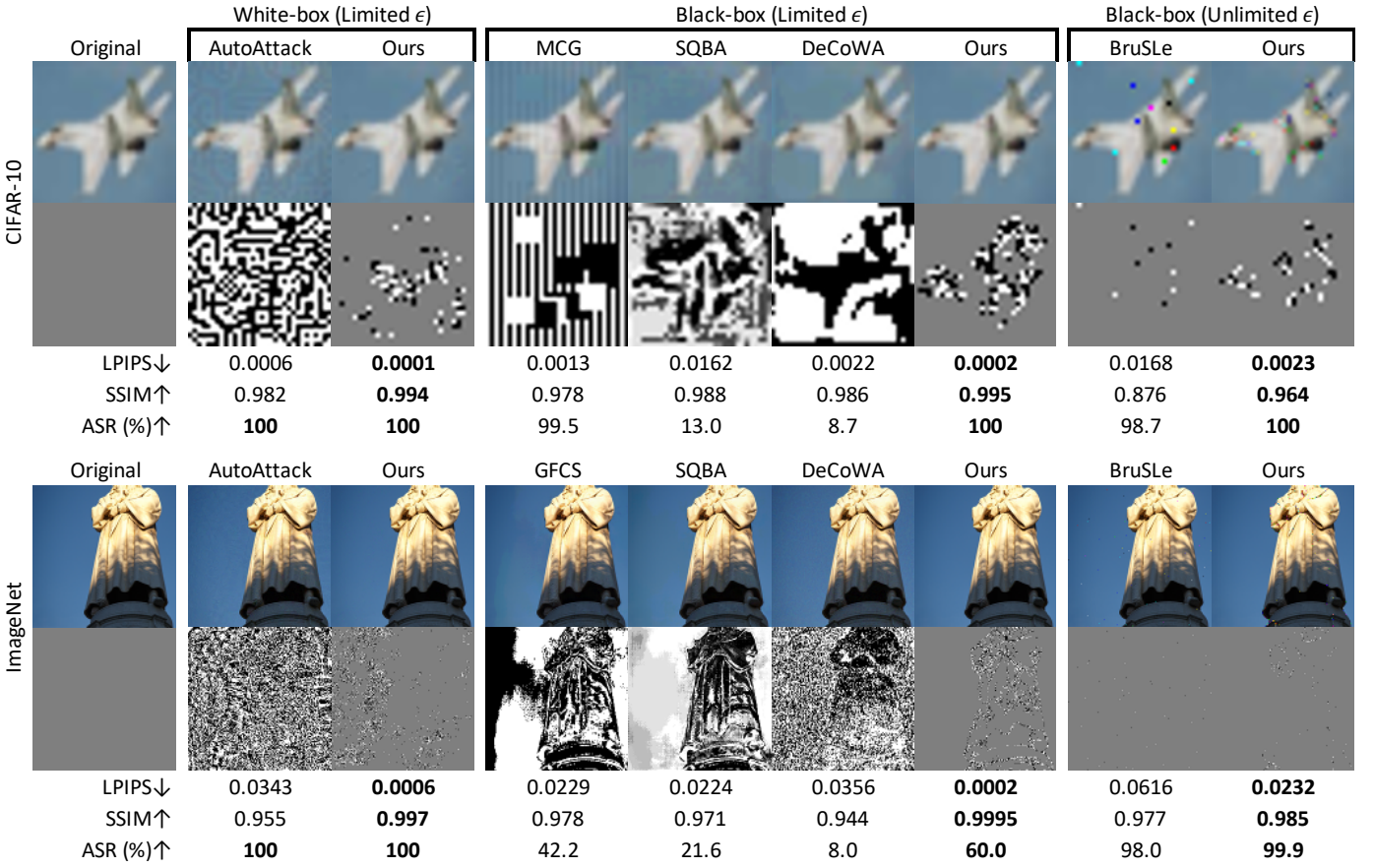


Fig. 4: Comparison of adversarial examples generated by different attack algorithms in terms of visual quality and perturbation appearance. The proposed GreedyPixel method achieved the highest visual quality by selectively modifying only critical pixels. The perturbations were normalized for visualization using Equation (23), with **bold** indicating superior performance. Notably, while the BruSLe attack [14] introduced fewer perturbed pixels than GreedyPixel, the visibility of these perturbations was higher due to their spatial placement.

these perturbations to compare the qualitative differences among algorithms, highlighting variations in visual quality. The grayscale perturbation illustration δ_{Gray} in Figure 4 was generated in two steps: first, the perturbations δ were normalized from the range $[\epsilon_{min}, \epsilon_{max}]$ to $[0, 1]$ to produce δ_{RGB} , and then δ_{RGB} was converted to grayscale using the NTSC formula [55]:

$$\begin{aligned} \delta_{RGB} &= \frac{\delta - \epsilon_{min}}{\epsilon_{max} - \epsilon_{min}}, \\ \delta_{Gray} &= 0.299 \cdot \delta_{RGB}.R + 0.587 \cdot \delta_{RGB}.G + 0.114 \cdot \delta_{RGB}.B, \end{aligned} \quad (23)$$

where $\delta_{RGB}.R$, $\delta_{RGB}.G$, and $\delta_{RGB}.B$ represent the red, green, and blue channels, respectively.

As shown in Tables II to V, GreedyPixel consistently outperformed the other attacks in visual quality, with higher SSIM and lower LPIPS scores. This is further demonstrated in Figure 4, where our method introduced less noticeable noise, especially in black-box settings. Similar to the BruSLe attack [14], GreedyPixel modified fewer pixels than methods such as AutoAttack [8], DeCoWA [20], GFCS [26], MCG [29], and SQBA [27], leading to more subtle and imperceptible changes. By focusing perturbations on robust features such as complex

TABLE VI: User study on visual quality.

Threat Model	Attack	CIFAR-10		ImageNet	
		ASR(%↑)	Invisible↑	ASR(%↑)	Invisible↑
White-box (Limited ϵ)	AutoAttack	100.0	32/50	100.0	38/50
	Ours	100.0	46/50	100.0	49/50
Black-box (Limited ϵ)	MCG	99.5	8/50	-	-
	GFCS	-	-	42.2	43/50
	Ours	100.0	47/50	60.0	49/50
Black-box (Unlimited ϵ)	BruSLe	98.7	0/50	98.0	2/50
	Ours	100.0	4/50	99.9	20/50

“Invisible” denotes percentage of examples with imperceptible perturbations. **Bold** indicates superior performance. MCG and GFCS did not release their code for ImageNet and CIFAR-10 datasets, respectively.

objects and edges, rather than the background, GreedyPixel achieved superior visual quality, making its perturbations minimally invasive yet highly effective.

D. User Study on Visual Quality

We conducted a user study to evaluate the human perceptual quality of adversarial examples. We randomly selected 100 original images and generated adversarial counterparts using

TABLE VII: Attack Performance (%) against adversarial defenses in counterattack experiments.

Threat Model	Attack	No Defense \uparrow	Purification ^a [50] \uparrow	AT [41] \uparrow	AT [42] \uparrow	AT [43] \uparrow	Detection ^b [51] \downarrow
White-box (Limited ϵ)	APGD	100.0	20.5	16.0	13.1	20.7	10.7
	AutoAttack	100.0	21.5	16.7	14.2	21.8	10.6
	GreedyPixel (ours)	100.0	25.4	16.5	14.0	21.4	8.4
Black-box (Limited ϵ)	DeCoWA ^c	8.7	16.2	9.9	9.0	13.4	7.7
	MCG	99.5	13.2	15.3	13.3	20.0	7.9
	SQBA	13.0	17.5	10.3	9.3	15.1	8.2
	GreedyPixel (ours)	100.0	23.4	16.4	14.0	21.3	8.5
Black-box (Unlimited ϵ)	BruSLe	98.7	30.8	72.5	75.5	57.1	81.9
	GreedyPixel (ours)	100.0	36.2	84.6	82.7	93.2	31.5

^aDiffusion timestep=0.1. ^bThe detector was trained on adversarial examples generated by Adversarial Patch [56], DeepFool [57], FGSM [4], PGD [6], APGD [8], Spatial Transformation [58], and Square [10] attacks. The threshold was set for a 5% clean rejection rate. ^cDeCoWA [20] demonstrated suboptimal performance when using the surrogate model [44] irrespective of whether it targeted non-robust or robust models. The higher ASR against DiffPure is attributable to distortion dominating over adversarial manipulations. **Bold** indicates superior performance.

seven methods: white-box AutoAttack [8], black-box GFCS [26] and MCG [29], sparse BruSLe [14], and GreedyPixel, under three threat models. The attacks were applied to the CIFAR-10 (low-resolution) and ImageNet (high-resolution) datasets. Thirty participants with varying vision levels were asked to identify adversarial examples that were indistinguishable from the originals. The samples were presented in random order to minimize bias.

As shown in Table VI, GreedyPixel achieved superior visual quality, with more adversarial examples judged indistinguishable from the originals, especially in white-box and black-box settings under limited ϵ . Under unlimited ϵ conditions, both GreedyPixel and BruSLe perturbations became more detectable, though GreedyPixel still outperformed BruSLe. Additionally, perturbations on CIFAR-10 were more easily detected than those on ImageNet, suggesting that high-resolution images present a greater challenge for defense mechanisms.

E. Effectiveness Against Adversarial Defenses

To assess GreedyPixel’s effectiveness under realistic deployment scenarios, we evaluated it against multiple representative defenses, including a state-of-the-art purification method (DiffPure [50]), three AT models [41]–[43] (including the top-ranked robust model [42] from RobustBench [38]), and an adversarial detector [51], using the CIFAR-10 dataset. The adversarial examples were generated using 20,000 queries without early stopping. As shown in Table VII, GreedyPixel outperformed the other methods, achieving comparable or higher ASRs and similar or lower adversarial detection rates across all three threat models. This demonstrates GreedyPixel’s enhanced effectiveness and adaptability in bypassing adversarial defenses.

F. Attacks Against Commercial Online Vision APIs

To further evaluate the real-world applicability of GreedyPixel, we conducted black-box attacks against two widely deployed commercial systems: Google Cloud Vision [59] and AWS Rekognition [60]. We used a subset of ImageNet samples as inputs and restricted the maximum query budget to 400, resulting in extremely sparse perturbations (< 0.1% pixels; *i.e.*, fewer than 50 pixels modified under unlimited ϵ).

As shown in Figure 5, GreedyPixel consistently reduced the confidence score of the correct class (sometimes to zero) within the tight budget. The qualitative results demonstrate that GreedyPixel generalizes beyond academic benchmarks and is highly effective in attacking real-world API-based vision models despite the limited number of queries and the practical constraints of commercial services. This highlights its practical relevance for assessing the robustness of deployed systems.

VI. ABLATION STUDY

A. Effect of Attack Constraint

We investigated the effect of increasing attack budgets. The visual quality comparisons in Figure 4 show that with a small L_∞ -norm constraint of 4/255, our method substantially outperformed others in SSIM and LPIPS scores. This indicates that increasing the attack budget can maintain superior visual quality while improving ASRs and attack efficiency. Figure 6 further supports this, showing that slight degradation in visual quality (as reflected in SSIM and LPIPS) can lead to improved attack efficiency and higher ASRs.

B. Maximum Query Limit

In query-based adversarial attacks, the maximum query limit markedly affects attack effectiveness, especially for challenging images. This limit is tied to the number of manipulable pixels, as described in Equation (9). The results of our analysis, summarized in Table VIII, illustrate the effects of varying the query limit across performance metrics. For example, setting a low query threshold (*e.g.*, 5,000 queries for CIFAR-10, equating to 625 pixels out of 1,024, or 20,000 queries for ImageNet, affecting 2,500 pixels out of 50,176) limits the number of pixels that can be altered, resulting in lower ASRs. However, increasing the threshold beyond 10,000 queries (1,250 pixels) for CIFAR-10 or 100,000 queries (12,500 pixels) for ImageNet leads to minimal improvements in effectiveness. In these higher-query settings, metrics such as Avg. Q, execution time, and perceptual measures like LPIPS and SSIM show little variation. This plateau effect occurs because the extra queries mainly affect previously unsuccessful cases, as seen in Figure 7. Moreover, ASRs in higher-query settings indicate that, with sufficient time and resources,

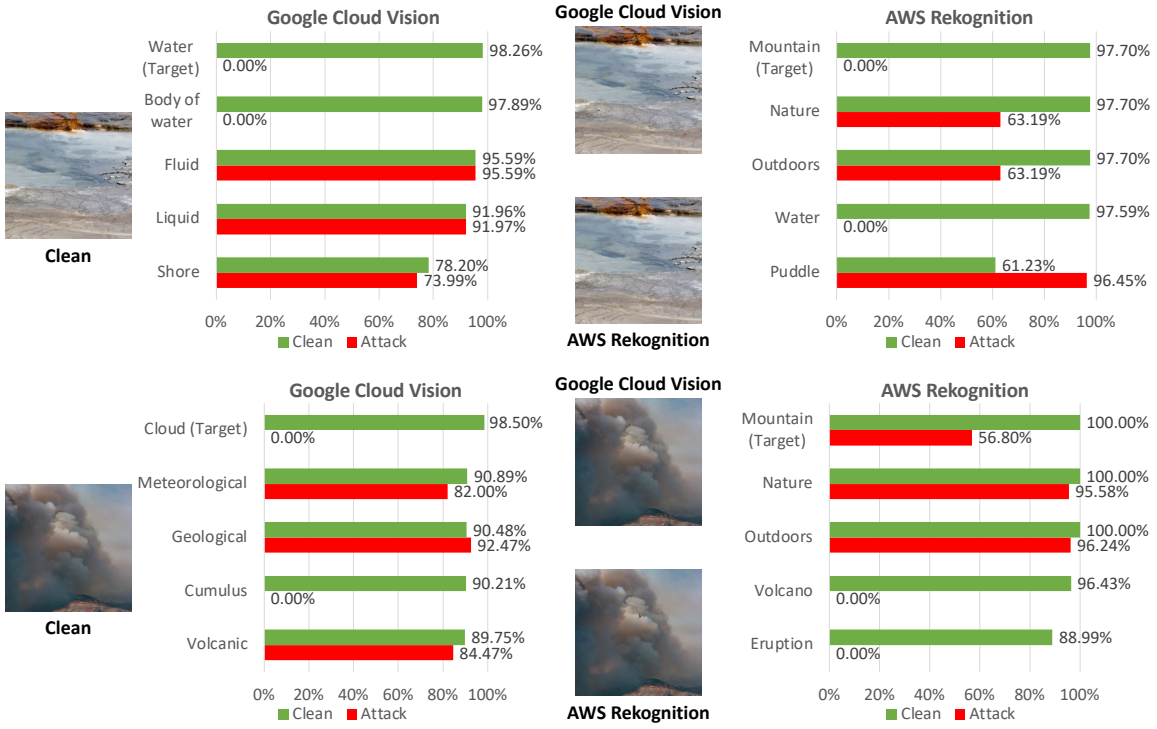


Fig. 5: Results of GreedyPixel attacks on commercial online vision APIs. Within a strict budget of 400 queries (perturbing fewer than 0.1% of pixels, *i.e.*, ≤ 50 pixels under unlimited ϵ), the confidence scores of the ground-truth class were significantly reduced—sometimes to zero. These results demonstrate that GreedyPixel remains effective even in real-world, production scenarios.

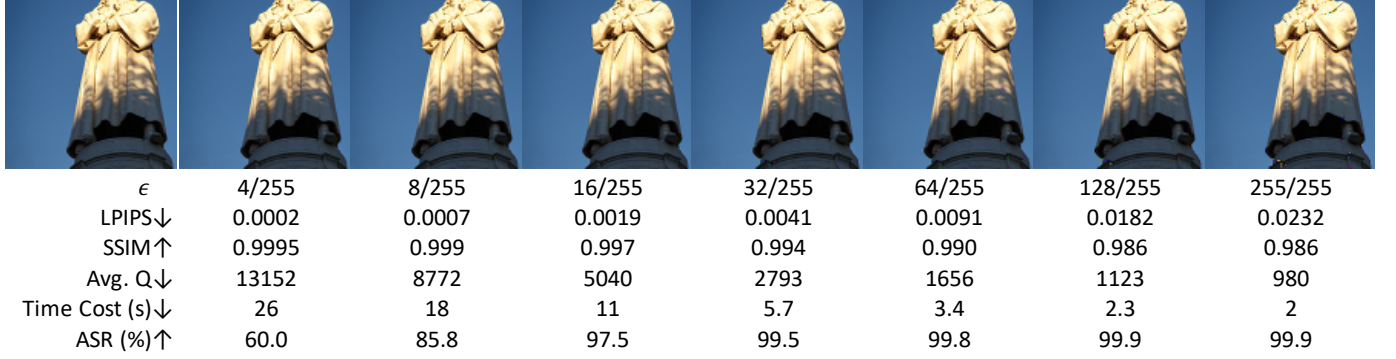


Fig. 6: Visual quality, efficiency, and ASRs under different L_∞ -norm attack budgets. GreedyPixel supports larger attack budgets, trading off slight degradation in visual quality (as measured by SSIM and LPIPS) for improved efficiency and higher ASRs.

GreedyPixel can achieve results comparable to gradient-based methods without requiring access to gradient information, as discussed in Section III-E.

C. Image Resolution

As shown in Table VIII, under an unconstrained query setting, ASRs approach 100% as image resolution increases, resulting in outcomes similar to those for low-resolution images, but at higher computational cost. However, under a constrained query budget, higher-resolution images lead to reduced ASRs, highlighting the increased difficulty GreedyPixel faces in attacking high-resolution images. These results demonstrate the

importance of an appropriate query budget that reflects the resolution of the images.

D. Periodicity of Updating Priority Map

We designed the priority map update frequency to improve visual quality of adversarial examples, as measured by LPIPS and SSIM, with a trade-off in ASR. By updating the map and resetting the adversary sequence to the most critical pixel, the attack was guided to focus on more important pixels. As shown in Table IX, increasing the update frequency (*i.e.*, reducing N in Algorithm 3) improved LPIPS and SSIM scores, indicating better visual quality, but reduced ASR. Additionally, we explored an alternative strategy in which sparsity was fixed by

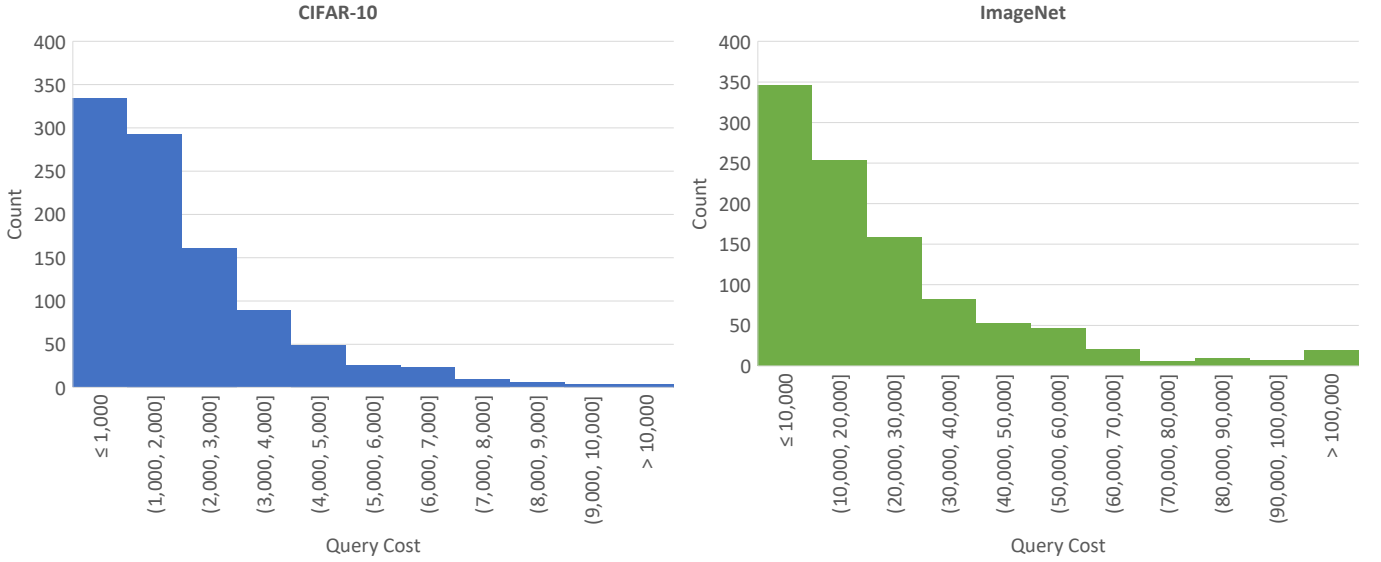


Fig. 7: Query costs and distribution of successful adversarial examples. This figure illustrates the distribution of query costs among successful adversarial examples, demonstrating that the majority of these examples require relatively few queries to succeed. While increasing the allowed number of queries can improve attack performance, the rate of improvement diminishes as the query limit grows larger. Beyond a certain point (10,000 queries / 1,250 pixels for CIFAR-10, or 100,000 queries / 12,500 pixels for ImageNet), further increases mainly affect the few remaining unsuccessful cases, leading to marginal gains in overall performance.

TABLE VIII: Black-box attack performance evaluation at a fixed perturbation limit of $\epsilon = 4/255$, under various maximum query constraints.

Resolution	Max. Q	Avg. Q \downarrow	Time (s) \downarrow	ASR (%) \uparrow	LPIPS \downarrow	SSIM \uparrow
32 \times 32 (CIFAR-10)	5K	1,863	1.7	92.6	0.0002	0.996
	10K	1,993	1.8	99.6	0.0002	0.995
	15K	1,997	1.8	100.0	0.0002	0.995
	20K	1,997	1.8	100.0	0.0002	0.995
64 \times 64 (ImageNet)	10K	2,687	4.7	94.9	0.0003	0.999
	20K	2,957	5.1	98.8	0.0003	0.999
	50K	3,108	5.5	99.7	0.0003	0.998
	100K	3,259	5.5	100.0	0.0003	0.998
224 \times 224 (ImageNet)	20K	13,152	26.4	60.0	0.0002	≈ 1
	50K	19,598	40.0	89.2	0.0004	0.999
	100K	21,816	44.4	98.1	0.0005	0.999
	200K	22,617	47.0	99.6	0.0005	0.999
	400K	23,003	47.1	99.9	0.0005	0.999

generating the priority map once and resetting the adversary sequence every N iterations. Such alternative improved visual quality but caused a substantial drop in ASR. Due to its lower practicality, we did not focus on this alternative.

E. Priority Map and Surrogate Models

We investigated the effect of using priority maps learned from different surrogate models, including two PreActResNet-18 variants [44], [45] and RaWideResNet-70-16 [46] for CIFAR-10, and ConvNeXt [47], Swin [48], and ResNet-18 [49] for ImageNet, which together represent a diverse range of architectures and robustness levels.

As shown in Table X, using the priority map noticeably improves attack efficiency, reducing average query count and exe-

TABLE IX: Performance of priority map updates across different periods, using WideResNet-28-10 [38] on CIFAR-10 [36].

Threat Model	Sparsity	Update Period	ASR (%) \uparrow	LPIPS \downarrow	SSIM \uparrow
White-box (Limited ϵ)	10%	Disable	50.3	≈ 0	0.997
	30%	Disable	90.3	≈ 0	0.995
	50%	Disable	98.6	0.0001	0.994
	Disable	$N = 100$	97.4	≈ 0	0.995
	Disable	$N = 300$	99.7	≈ 0	0.994
	Disable	$N = 500$	100.0	0.0001	0.994
Black-box (Limited ϵ)	Disable	Disable	100.0	0.0001	0.994
	10%	Disable	29.9	≈ 0	0.998
	30%	Disable	86.1	0.0001	0.997
	50%	Disable	97.6	0.0002	0.996
	Disable	$N = 100$	40.0	≈ 0	0.998
	Disable	$N = 300$	91.6	0.0001	0.996
	Disable	$N = 500$	98.8	0.0002	0.996
	Disable	Disable	100.0	0.0002	0.995

Bold indicates superior performance.

cution time compared with the “Random” approach, especially under query constraints (e.g., for high-resolution images like those in ImageNet). “White-box” knowledge further enhances both effectiveness and efficiency by leveraging precise gradient information. Additionally, adversarially trained models used as surrogates improve the visual quality compared with non-robust models, although the gains are modest.

These findings are illustrated in Figure 8, which shows that the priority map accelerates convergence by reducing the number of queries required to achieve loss values comparable to those with the “Random” approach. The “White-box” curves reflect superior performance, reinforcing the value of our strategy, particularly for high-resolution images, for which query efficiency is a critical factor.

TABLE X: Attack performance with a fixed perturbation limit of $\epsilon = 4/255$ and a maximum query budget of 20,000 (including white-box attacks), evaluated across various surrogate models.

Dataset	Target Model	Surrogate Model	Avg. Q \downarrow	Time (s) \downarrow	ASR (%) \uparrow	LPIPS \downarrow	SSIM \uparrow
CIFAR-10	WideResNet-28-10 [38]	WideResNet-28-10 [38] ^a	1,510	1.3	100.0	0.0001	0.994
		PreActResNet-18 [44]	1,997	1.8	100.0	0.0002	0.995
		PreActResNet-18 [45]	2,052	1.8	100.0	0.0002	0.995
		RaWideResNet-70-16 [46]	2,040	1.8	100.0	0.0002	0.995
		Random ^b	2,220	2.1	100.0	0.0001	0.994
ImageNet	ResNet-50 [38]	ResNet-50 [38] ^a	7,826	16.4	86.1	0.0005	0.997
		ConvNeXt [47]	13,152	26.1	60.0	0.0002	≈ 1
		Swin [48]	13,242	27.0	59.2	0.0003	0.999
		ResNet-18 [49]	13,563	27.1	57.6	0.0002	0.999
		Random ^b	14,149	27.4	54.9	0.0004	0.997

^aDenotes white-box attacks where surrogate model was identical to target model. ^bDenotes use of random map with no priority calculation for pixel selection.

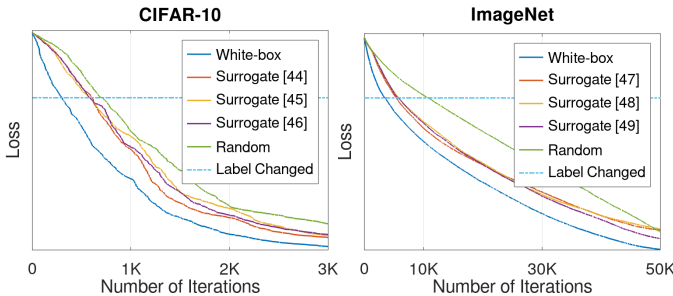


Fig. 8: Query efficiency of proposed pixel-wise priority map under black-box and white-box settings. The proposed pixel-wise priority map effectively reduces the number of queries, with potential for further enhancement when incorporating white-box knowledge.

VII. DISCUSSION OF ALTERNATIVE STRATEGIES

We have demonstrated that the priority map is crucial for efficiency. Although GreedyPixel achieves strong performance, its query cost increases with image resolution, posing a computational challenge for very high-resolution inputs.

One potential approach is to simply increase the query budget until success is achieved. However, this is often impractical due to a long execution time, the risk of query blocking in deployed systems, and the resulting degradation of visual quality caused by excessive perturbations.

Another direction is to explore alternative priority maps, such as region-, objective-, edge-, or attention-based maps. While these approaches group pixels with the same priority, they require processing all pixels within each group, which typically reduces efficiency compared with per-pixel ordering. Our ablation study described in Section VI-D demonstrated that re-ranking frequency plays an important role in balancing visual quality and attack success, suggesting that adaptive scheduling of priority refresh may further improve efficiency.

Given current knowledge, we believe that our algorithm represents an optimal compromise: it guarantees monotonic loss decrease, preserves high perceptual quality, and maintains query efficiency. Nevertheless, reducing query cost for very high-resolution images remains an open problem, and we plan to investigate advanced solutions such as hierarchical pixel selection and gradient-free attention guidance in future work.

VIII. CONCLUSION AND FUTURE RESEARCH

We have presented the strongest black-box adversarial attack to date, *GreedyPixel*, which achieves robustness near that of white-box attacks without requiring gradient information. It is based on a novel strategy for black-box learning that supports fine-grained manipulations and provides precise control. By simulating white-box-like optimization while overcoming the local optima limitations of gradient descent, GreedyPixel bridges the gap between black-box and white-box learning. By leveraging a greedy algorithm and priority map, our approach makes brute-force adversarial learning feasible with a reasonable computational cost, achieving near-global optimality without gradient reliance. This advancement enhances both adversarial learning and general optimization techniques.

Future work will explore alternative approaches to constructing the priority map to further enhance the efficiency of greedy learning. Additionally, we will demonstrate the applicability of GreedyPixel for manipulating sensitive entities, such as the latent codes of diffusion models, to achieve precise image editing under black-box conditions.

REFERENCES

- [1] J. Deng, J. Guo, N. Xue, and S. Zafeiriou, “Arcface: Additive angular margin loss for deep face recognition,” in *Proceedings of the IEEE/CVF Conference on Computer Vision and Pattern Recognition (CVPR)*, pp. 4690–4699, 2019.
- [2] X. Liu, L. Faes, A. U. Kale, S. K. Wagner, D. J. Fu, A. Bruynseels, T. Mahendiran, G. Moraes, M. Shamdas, C. Kern, *et al.*, “A comparison of deep learning performance against health-care professionals in detecting diseases from medical imaging: a systematic review and meta-analysis,” *The lancet digital health*, vol. 1, no. 6, pp. e271–e297, 2019.
- [3] A. Radford, J. W. Kim, C. Hallacy, A. Ramesh, G. Goh, S. Agarwal, G. Sastry, A. Askell, P. Mishkin, J. Clark, *et al.*, “Learning transferable visual models from natural language supervision,” in *International conference on machine learning (ICML)*, pp. 8748–8763, PMLR, 2021.
- [4] I. J. Goodfellow, J. Shlens, and C. Szegedy, “Explaining and harnessing adversarial examples,” *arXiv preprint arXiv:1412.6572*, 2014.
- [5] N. Carlini and D. Wagner, “Towards evaluating the robustness of neural networks,” in *2017 IEEE Symposium on Security and Privacy (S&P)*, pp. 39–57, 2017.
- [6] A. Madry, A. Makelov, L. Schmidt, D. Tsipras, and A. Vladu, “Towards deep learning models resistant to adversarial attacks,” in *International Conference on Learning Representations (ICLR)*, 2018.
- [7] X. Dong, D. Chen, J. Bao, C. Qin, L. Yuan, W. Zhang, N. Yu, and D. Chen, “Greedyfool: Distortion-aware sparse adversarial attack,” *Advances in Neural Information Processing Systems (NeurIPS)*, vol. 33, pp. 11226–11236, 2020.
- [8] F. Croce and M. Hein, “Reliable evaluation of adversarial robustness with an ensemble of diverse parameter-free attacks,” in *International Conference on Machine Learning (ICML)*, pp. 2206–2216, 2020.

[9] S. Moon, G. An, and H. O. Song, "Parsimonious black-box adversarial attacks via efficient combinatorial optimization," in *International Conference on Machine Learning (ICML)*, pp. 4636–4645, PMLR, 2019.

[10] M. Andriushchenko, F. Croce, N. Flammarion, and M. Hein, "Square attack: a query-efficient black-box adversarial attack via random search," in *European Conference on Computer Vision (ECCV)*, pp. 484–501, 2020.

[11] L. Wang, K. Yang, W. Wang, R. Wang, and A. Ye, "Mgaattack: Toward more query-efficient black-box attack by microbial genetic algorithm," in *Proceedings of the 28th ACM International Conference on Multimedia (ACM MM)*, pp. 2229–2236, 2020.

[12] C. Wu, W. Luo, N. Zhou, P. Xu, and T. Zhu, "Genetic algorithm with multiple fitness functions for generating adversarial examples," in *2021 IEEE Congress on Evolutionary Computation (CEC)*, pp. 1792–1799, IEEE, 2021.

[13] J. Su, D. V. Vargas, and K. Sakurai, "One pixel attack for fooling deep neural networks," *IEEE Transactions on Evolutionary Computation*, vol. 23, no. 5, pp. 828–841, 2019.

[14] Q. V. Vo, E. Abbasnejad, and D. Ranasinghe, "Brusleattack: Query-efficient score-based sparse adversarial attack," in *The Twelfth International Conference on Learning Representations (ICLR)*, 2024.

[15] C. Luo, Q. Lin, W. Xie, B. Wu, J. Xie, and L. Shen, "Frequency-driven imperceptible adversarial attack on semantic similarity," in *Proceedings of the IEEE/CVF Conference on Computer Vision and Pattern Recognition (CVPR)*, pp. 15315–15324, 2022.

[16] Y. Long, Q. Zhang, B. Zeng, L. Gao, X. Liu, J. Zhang, and J. Song, "Frequency domain model augmentation for adversarial attack," in *European Conference on Computer Vision (ECCV)*, pp. 549–566, Springer, 2022.

[17] Y. Wang, Y. Wu, S. Wu, X. Liu, W. Zhou, L. Zhu, and C. Zhang, "Boosting the transferability of adversarial attacks with frequency-aware perturbation," *IEEE Transactions on Information Forensics and Security*, vol. 19, pp. 6293–6304, 2024.

[18] H. Cao, Q. Sun, Y. Li, R. Geng, and X. Wang, "Efficient history-driven adversarial perturbation distribution learning in low frequency domain," *ACM Transactions on Privacy and Security*, vol. 27, no. 1, pp. 1–25, 2024.

[19] Z. Wang, H. Guo, Z. Zhang, W. Liu, Z. Qin, and K. Ren, "Feature importance-aware transferable adversarial attacks," in *Proceedings of the IEEE/CVF International Conference on Computer Vision (ICCV)*, pp. 7639–7648, 2021.

[20] Q. Lin, C. Luo, Z. Niu, X. He, W. Xie, Y. Hou, L. Shen, and S. Song, "Boosting adversarial transferability across model genus by deformation-constrained warping," in *Proceedings of the AAAI Conference on Artificial Intelligence (AAAI)*, pp. 3459–3467, 2024.

[21] Y. Guo, W. Liu, Q. Xu, S. Zheng, S. Huang, Y. Zang, S. Shen, C. Wen, and C. Wang, "Boosting adversarial transferability through augmentation in hypothesis space," in *Proceedings of the Computer Vision and Pattern Recognition Conference (CVPR)*, pp. 19175–19185, 2025.

[22] F. Gan and Y. Wo, "Boosting the transferability of adversarial examples through gradient aggregation," *IEEE Transactions on Information Forensics and Security*, vol. 20, pp. 5563–5576, 2025.

[23] Y. Qian, S. He, C. Zhao, J. Sha, W. Wang, and B. Wang, "Lea2: A lightweight ensemble adversarial attack via non-overlapping vulnerable frequency regions," in *Proceedings of the IEEE/CVF International Conference on Computer Vision (ICCV)*, pp. 4510–4521, 2023.

[24] Y. Qian, K. Chen, B. Wang, Z. Gu, S. Ji, W. Wang, and Y. Zhang, "Enhancing transferability of adversarial examples through mixed-frequency inputs," *IEEE Transactions on Information Forensics and Security*, 2024.

[25] Z. Cai, C. Song, S. Krishnamurthy, A. Roy-Chowdhury, and S. Asif, "Blackbox attacks via surrogate ensemble search," *Advances in Neural Information Processing Systems (NeurIPS)*, vol. 35, pp. 5348–5362, 2022.

[26] N. A. Lord, R. Mueller, and L. Bertinetto, "Attacking deep networks with surrogate-based adversarial black-box methods is easy," in *International Conference on Learning Representations (ICLR)*, 2022.

[27] J. Park, P. Miller, and N. McLaughlin, "Hard-label based small query black-box adversarial attack," in *Proceedings of the IEEE/CVF Winter Conference on Applications of Computer Vision (WACV)*, pp. 3986–3995, 2024.

[28] Y. Feng, B. Wu, Y. Fan, L. Liu, Z. Li, and S.-T. Xia, "Boosting black-box attack with partially transferred conditional adversarial distribution," in *Proceedings of the IEEE/CVF Conference on Computer Vision and Pattern Recognition (CVPR)*, pp. 15095–15104, 2022.

[29] F. Yin, Y. Zhang, B. Wu, Y. Feng, J. Zhang, Y. Fan, and Y. Yang, "Generalizable black-box adversarial attack with meta learning," *IEEE Transactions on Pattern Analysis and Machine Intelligence*, 2023.

[30] J. Liu, J. Zhou, J. Zeng, and J. Tian, "Difattack: Query-efficient black-box adversarial attack via disentangled feature space," in *Proceedings of the AAAI Conference on Artificial Intelligence (AAAI)*, pp. 3666–3674, 2024.

[31] R. Liu, W. Zhou, T. Zhang, K. Chen, J. Zhao, and K.-Y. Lam, "Boosting black-box attack to deep neural networks with conditional diffusion models," *IEEE Transactions on Information Forensics and Security*, vol. 19, pp. 5207–5219, 2024.

[32] Y. Bengio, P. Simard, and P. Frasconi, "Learning long-term dependencies with gradient descent is difficult," *IEEE Transactions on Neural Networks*, vol. 5, no. 2, pp. 157–166, 1994.

[33] G. E. Hinton, S. Osindero, and Y.-W. Teh, "A fast learning algorithm for deep belief nets," *Neural Computation*, vol. 18, no. 7, pp. 1527–1554, 2006.

[34] F. Tramèr, A. Kurakin, N. Papernot, I. Goodfellow, D. Boneh, and P. McDaniel, "Ensemble adversarial training: Attacks and defenses," in *International Conference on Learning Representations (ICLR)*, 2018.

[35] R. Motwani and P. Raghavan, *Randomized Algorithms*. Cambridge University Press, 1995.

[36] A. Krizhevsky, G. Hinton, *et al.*, "Learning multiple layers of features from tiny images," tech. rep., University of Toronto, 2009.

[37] I. G. Alex K, Ben Hamner, "Nips 2017: Defense against adversarial attack." <https://kaggle.com/competitions/nips-2017-defense-against-adversarial-attack>, 2017. Accessed: 2025-11-09.

[38] F. Croce, M. Andriushchenko, V. Sehwag, E. Debenedetti, N. Flammarion, M. Chiang, P. Mittal, and M. Hein, "Robustbench: a standardized adversarial robustness benchmark," in *Thirty-fifth Conference on Neural Information Processing Systems Datasets and Benchmarks Track (Round 2) (NeurIPS 2021)*, 2021.

[39] B. Wu, C. Xu, X. Dai, A. Wan, P. Zhang, Z. Yan, M. Tomizuka, J. Gonzalez, K. Keutzer, and P. Vajda, "Visual transformers: Token-based image representation and processing for computer vision," *arXiv preprint arXiv:2006.03677*, 2020.

[40] K. Simonyan and A. Zisserman, "Very deep convolutional networks for large-scale image recognition," in *3rd International Conference on Learning Representations (ICLR)*, Computational and Biological Learning Society, 2015.

[41] Z. Wang, T. Pang, C. Du, M. Lin, W. Liu, and S. Yan, "Better diffusion models further improve adversarial training," in *International Conference on Machine Learning (ICML)*, pp. 36246–36263, PMLR, 2023.

[42] B. R. Bartoldson, J. Diffenderfer, K. Parasyris, and B. Kailkhura, "Adversarial robustness limits via scaling-law and human-alignment studies," in *International Conference on Machine Learning (ICML)*, pp. 3046–3072, PMLR, 2024.

[43] E. Debenedetti, V. Sehwag, and P. Mittal, "A light recipe to train robust vision transformers," in *2023 IEEE Conference on Secure and Trustworthy Machine Learning (SaTML)*, pp. 225–253, 2023.

[44] E. Wong, L. Rice, and J. Z. Kolter, "Fast is better than free: Revisiting adversarial training," in *International Conference on Learning Representations (ICLR)*, 2020.

[45] S. Gowal, S.-A. Rebuffi, O. Wiles, F. Stimberg, D. A. Calian, and T. A. Mann, "Improving robustness using generated data," *Advances in Neural Information Processing Systems (NeurIPS)*, vol. 34, pp. 4218–4233, 2021.

[46] S. Peng, W. Xu, C. Cornelius, M. Hull, K. Li, R. Duggal, M. Phute, J. Martin, and D. H. Chau, "Robust principles: Architectural design principles for adversarially robust cnns," *arXiv preprint arXiv:2308.16258*, 2023.

[47] N. D. Singh, F. Croce, and M. Hein, "Revisiting adversarial training for imagenet: Architectures, training and generalization across threat models," *arXiv preprint arXiv:2303.01870*, 2023.

[48] C. Liu, Y. Dong, W. Xiang, X. Yang, H. Su, J. Zhu, Y. Chen, Y. He, H. Xue, and S. Zheng, "A comprehensive study on robustness of image classification models: Benchmarking and rethinking," *arXiv preprint arXiv:2302.14301*, 2023.

[49] H. Salman, A. Ilyas, L. Engstrom, A. Kapoor, and A. Madry, "Do adversarially robust imagenet models transfer better?," *Advances in Neural Information Processing Systems (NeurIPS)*, vol. 33, pp. 3533–3545, 2020.

[50] W. Nie, B. Guo, Y. Huang, C. Xiao, A. Vahdat, and A. Anandkumar, "Diffusion models for adversarial purification," in *International Conference on Machine Learning (ICML)*, pp. 16805–16827, 2022.

[51] D. Meng and H. Chen, "Magnet: a two-pronged defense against adversarial examples," in *Proceedings of the 2017 ACM SIGSAC Conference*

on Computer and Communications Security (ACM CCS), pp. 135–147, 2017.

[52] Z. Wang, A. C. Bovik, H. R. Sheikh, and E. P. Simoncelli, “Image quality assessment: from error visibility to structural similarity,” *IEEE Transactions on Image Processing*, vol. 13, no. 4, pp. 600–612, 2004.

[53] R. Zhang, P. Isola, A. A. Efros, E. Shechtman, and O. Wang, “The unreasonable effectiveness of deep features as a perceptual metric,” in *Proceedings of the IEEE Conference on Computer Vision and Pattern Recognition (CVPR)*, pp. 586–595, 2018.

[54] M.-I. Nicolae, M. Sinn, M. N. Tran, B. Buesser, A. Rawat, M. Wistuba, V. Zantedeschi, N. Baracaldo, B. Chen, H. Ludwig, I. Molloy, and B. Edwards, “Adversarial robustness toolbox v1.2.0,” *CoRR*, 2018.

[55] D. Livingston, “Colorimetric analysis of the ntsc color television system,” *Proceedings of the IRE*, vol. 42, no. 1, pp. 138–150, 1954.

[56] T. B. Brown, D. Mané, A. Roy, M. Abadi, and J. Gilmer, “Adversarial patch,” *arXiv preprint arXiv:1712.09665*, 2017.

[57] S.-M. Moosavi-Dezfooli, A. Fawzi, and P. Frossard, “Deepfool: a simple and accurate method to fool deep neural networks,” in *Proceedings of the IEEE Conference on Computer Vision and Pattern Recognition (CVPR)*, pp. 2574–2582, 2016.

[58] C. Xiao, J.-Y. Zhu, B. Li, W. He, M. Liu, and D. Song, “Spatially transformed adversarial examples,” in *International Conference on Learning Representations (ICLR)*, 2018.

[59] Google Cloud, “Google cloud vision api documentation.” <https://cloud.google.com/vision>, 2025. Accessed: 2025-09-09.

[60] Amazon Web Services, “Amazon rekognition api documentation.” <https://docs.aws.amazon.com/rekognition>, 2025. Accessed: 2025-09-09.



Hanrui Wang received his B.S. degree in Electronic Information Engineering from Northeastern University (China) in 2011. He left the IT industry from a director position in 2019 to pursue a research career and received his Ph.D. in Computer Science from Monash University, Australia, in January 2024. He is currently working as a Postdoctoral Researcher with the Echizen Laboratory at the National Institute of Informatics (NII) in Tokyo, Japan. His research interests include AI security and privacy, particularly adversarial machine learning.



Ching-Chun Chang received the PhD in Computer Science from the University of Warwick, UK, in 2019. He is currently a Project Assistant Professor with the National Institute of Informatics, Japan. He participated in a short-term scientific mission supported by European Cooperation in Science and Technology Actions at the Faculty of Computer Science, Otto von Guericke University of Magdeburg, Germany, in 2016. He was granted the Marie-Curie fellowship and participated in a research and innovation staff exchange scheme supported by Marie Skłodowska-Curie Actions at the Department of Electrical and Computer Engineering, New Jersey Institute of Technology, USA, in 2017. He was a Visiting Scholar with the School of Computer and Mathematics, Charles Sturt University, Australia, in 2018, and with the School of Information Technology, Deakin University, Australia, in 2019. He was a Research Fellow with the Department of Electronic Engineering, Tsinghua University, China, in 2020. His research interests include artificial intelligence, biometrics, cryptography, cybernetics, cybersecurity, forensics, information theory, mathematical optimisation, steganography, and watermarking.



Chun-Shien Lu received the Ph.D. degree in Electrical Engineering from National Cheng-Kung University, Tainan, Taiwan in 1998. He is a full research fellow (full professor) in the Institute of Information Science since March 2013 and the executive director in the Taiwan Information Security Center, Research Center for Information Technology Innovation, Academia Sinica, Taipei, Taiwan, since June 2024. His current research interests mainly focus on deep learning, AI security and privacy, and inverse problems. Dr. Lu serves as a Technical Committee member of Communications and Information Systems Security (CIS-TC) and Multimedia Communications Technical Committee (MMTC), IEEE Communications Society, since 2012 and 2017, respectively. Dr. Lu also serves as Area Chairs of ICASSP 2012–2014, ICIP 2013, ICME 2018, ICIP 2019–2025, ICML 2020, ICML 2023–2025, ICLR 2021–2026, NeurIPS 2022–2025, and ACM Multimedia 2022–2025, and Senior program committee of AAAI 2025–2026. Dr. Lu has owned four US patents, five ROC patents, and one Canadian patent in digital watermarking and graphic QR code. Dr. Lu won Ta-You Wu Memorial Award, National Science Council in 2007 and was a co-recipient of a National Invention and Creation Award in 2004. Dr. Lu was an associate editor of IEEE Trans. on Image Processing from 2010/12 to 2014 and from 2018/3 to 2023/6.



Christopher Leckie is currently a Professor with the School of Computing and Information Systems, The University of Melbourne. His research interests include artificial intelligence (AI), machine learning, anomaly detection, unsupervised learning, telecommunications, and cybersecurity. He has a strong interest in developing AI and machine learning techniques for a variety of applications in telecommunications, such as cyber security, network management, fault diagnosis, and the Internet of Things. He also has an interest in robust and scalable machine learning algorithms for problems, such as clustering and anomaly detection, with a focus on adversarial machine learning and security analytics.



Isao Echizen (Senior Member, IEEE) received B.S., M.S., and D.E. degrees from the Tokyo Institute of Technology, Japan, in 1995, 1997, and 2003, respectively. He joined Hitachi, Ltd. in 1997 and until 2007 was a research engineer in the company’s systems development laboratory. He is currently a director and a professor of the Information and Society Research Division, the National Institute of Informatics (NII), a director of the Global Research Center for Synthetic Media, the NII, a professor in the Department of Information and Communication Engineering, Graduate School of Information Science and Technology, the University of Tokyo, and a professor in the Graduate Institute for Advanced Studies, the Graduate University for Advanced Studies (SOKENDAI), Japan. He was a visiting professor at the University of Freiburg, Germany, and at the University of Halle-Wittenberg, Germany. He is currently engaged in research on AI security, multimedia security, and multimedia forensics. He is a research director in the CREST FakeMedia project and in the K Program SYNTHETIQ X, Japan Science and Technology Agency (JST). He received the Commendation for Science and Technology by the Minister of Education, Culture, Sports, Science and Technology (Research category) in 2025, the Best Paper Award from the IEICE in 2023, the Best Paper Awards from the IPSJ in 2005 and 2014, the IPSJ Nagao Special Researcher Award in 2011, the DOCOMO Mobile Science Award in 2014, the Information Security Cultural Award in 2016, and the IEEE Workshop on Information Forensics and Security Best Paper Award in 2017. He was a member of the Information Forensics and Security Technical Committee of the IEEE Signal Processing Society. He is the IEICE Fellow, the IPSJ Fellow, the IEEE Senior Member, and the Japanese representative on IFIP and on IFIP TC11 (Security and Privacy Protection in Information Processing Systems), a vice president of APSIPA, and an editorial board member of the IEEE Transactions on Dependable and Secure Computing, the EURASIP Journal on Image and Video Processing, and the Journal of Information Security and Applications, Elsevier.

APPENDIX A EVALUATION METRICS

A. Attack Success Rate (ASR)

The ASR quantifies the effectiveness of an adversarial attack in altering the model's prediction. It is defined as the proportion of AEs that successfully cause the model to produce incorrect predictions. Mathematically, it can be expressed as:

$$ASR = \frac{\text{Number of successful AEs}}{\text{Number of All AEs}}. \quad (24)$$

A higher ASR indicates a more effective attack, as it reflects the ability of the AEs to mislead the model.

B. Adversarial Detection Rate

The adversarial detection rate refers to the proportion of AEs that are correctly identified by an adversarial detector. It is defined as:

$$\text{Detection Rate} = \frac{\text{Number of AEs detected}}{\text{Number of All AEs}}. \quad (25)$$

A lower detection rate indicates higher attack efficacy, as it reflects the ability of the AEs to evade detection.

C. Structural Similarity Index (SSIM)

The SSIM is a metric for measuring similarity between two images. It considers luminance, contrast, and structural information. The SSIM between two images x (reference) and y (distorted) is defined as:

$$SSIM(x, y) = \frac{(2\mu_x\mu_y + C_1)(2\sigma_{xy} + C_2)}{(\mu_x^2 + \mu_y^2 + C_1)(\sigma_x^2 + \sigma_y^2 + C_2)}, \quad (26)$$

where:

- μ_x and μ_y : Mean intensity values of x and y , respectively.
- σ_x^2 and σ_y^2 : Variance of x and y , respectively.
- σ_{xy} : Covariance between x and y .
- C_1 and C_2 : Small constants added to stabilize the metric in the presence of weak denominators, defined as:

$$C_1 = (K_1 L)^2, \quad C_2 = (K_2 L)^2, \quad (27)$$

where L is the dynamic range of the pixel values (e.g., 255 for 8-bit images), and K_1 and K_2 are small positive constants (commonly, $K_1 = 0.01$ and $K_2 = 0.03$).

The SSIM value ranges from -1 to 1, where:

- 1: Perfect similarity.
- 0: No similarity.
- Negative values indicate dissimilarity.

SSIM is typically calculated locally using a sliding window across the image, and the overall SSIM is the average of local SSIM values. Higher SSIM values denote subtler deviations from the reference images.

D. Learned Perceptual Image Patch Similarity (LPIPS)

The LPIPS is a perceptual similarity measure that evaluates the perceptual distance between two images. It uses deep neural network features to compare the visual content and correlates better with human perception than traditional metrics like SSIM.

The LPIPS distance between two images x (reference) and y (distorted) is computed as:

$$LPIPS(x, y) = \sum_l \frac{1}{H_l W_l} \sum_{h=1}^{H_l} \sum_{w=1}^{W_l} w_l \|\hat{\phi}_l(x)_{h,w} - \hat{\phi}_l(y)_{h,w}\|_2^2, \quad (28)$$

where:

- l : Layer index in the deep network.
- $\hat{\phi}_l(x)$: Feature map of x at layer l in the network.
- $\hat{\phi}_l$: Normalized feature maps for each channel.
- H_l, W_l : Height and width of the feature map at layer l .
- w_l : Learned scalar weights for each layer l (trained to match human judgments).

LPIPS uses a pretrained deep neural network to extract feature maps from intermediate layers. The metric normalizes the feature maps and computes the difference between them, weighted according to the learned weights w_l . The LPIPS value typically ranges from 0 (perfect perceptual similarity) to higher values indicating greater dissimilarity. LPIPS provides a perceptually grounded comparison, making it especially useful for evaluating subtle changes in visual quality.

APPENDIX B EXPERIMENT SETTINGS

The complete attack configurations are summarized in Table XI, and all evaluated models are presented in Table XII.

APPENDIX C DISCUSSION

A. Actual Perturbation Values Applied to Effective Adversarial Examples

Table XIII summarizes our analysis of 1,000 adversarial examples produced by AutoAttack [8]. We observe that 70.43% of perturbation components under the L_∞ threat model assume the extreme values $\pm\epsilon$, indicating that successful attacks

TABLE XI: Attack Settings.

Threat Model	Attack	Max. Q	ϵ	Sparsity
White-Box (Limited ϵ)	APGD [8] AutoAttack [8] GreedyPixel (Ours)	Unlimited	4/255	N/A
Black-Box (Limited ϵ)	DeCoW [20] MCG [29] GFCS [26] SQBA [27] GreedyPixel (Ours)	20,000	4/255	N/A
Black-Box (Unlimited ϵ)	BruSLE [14] GreedyPixel (Ours)	20,000	Unlimited	1%/0.1%* N/A

*The sparsity for attacking CIFAR-10 and ImageNet was set to 1% (10 pixels) and 0.1% (50 pixels), respectively.

TABLE XII: Model architectures.

Dataset	Architecture	Role	Adversarial Training?
CIFAR-10	WideResNet-28-10 [38]	Target	NO
	WideResNet-28-10 [41]	Target	YES
	WideResNet-82-8 [42]	Target	YES
	XCiT-S12 [43]	Target	YES
	PreActResNet-18 [44]	Surrogate	YES
	PreActResNet-18 [45]*	Surrogate	YES
	RaWideResNet-70-16 [46]*	Surrogate	YES
ImageNet	ResNet-50 [38]	Target	NO
	ViT-Base-Patch16 [39]	Target	NO
	VGG19-BN [40]	Target	NO
	ConvNeXt [47]	Surrogate	YES
	Swin [48]*	Surrogate	YES
	ResNet-18 [49]*	Surrogate	YES

* denotes the surrogate model was assessed for ablation studies only.

TABLE XIII: The ratio (%) of perturbation values (in terms of their absolute values) in effective AEs @ L_∞ -norm $\epsilon = 4/255$.

Value	CIFAR-10	ImageNet	Average
4/255	70.43	42.23	56.330
3/255	8.40	18.47	13.435
2/255	6.46	13.59	10.025
1/255	6.14	12.51	9.325
0	8.57	13.2	10.885

Bold denotes the largest proportion.



Fig. 9: Model-inversion attack generations from the same source image to the same target image. Square [10] and BruSLe [14] attacks introduce significant differences.

frequently exploit the perturbation bounds. Motivated by this empirical finding, GreedyPixel constrains the search space to $\pm\epsilon$ per pixel and thereby reduces the combinatorial brute-force problem to a tractable pixel-wise greedy optimization.

B. Manipulation on Sensitive Entities

Our recent work emphasizes the critical importance of fine-grained manipulations, like our GreedyPixel attack, particularly when targeting sensitive entities such as the latent codes in diffusion models. In contrast, other black-box methods, including Square [10] and BruSLe [14] attacks, often produce noticeable distortions or noise during the generation process, as illustrated in Figure 9.